IMPROVED DROUGHT EARLY WARNING AND FORECASTING TO STRENGTHEN PREPAREDNESS AND ADAPTATION TO DROUGHTS IN AFRICA

DEWFORA

A 7th Framework Programme Collaborative Research Project

Potential to supplementing drought early warning systems with new meteorological information

WP4-D.4.4

October 2012

Coordinator: Deltares, The Netherlands
Project website: www.dewfora.net
FP7 Call ENV-2010-1.3.3.1
Contract no. 265454

Page intentionally left blank

DOCUMENT INFORMATION

Title	Report on the potential to supplementing drought early warning systems with new meteorological information and indices for the Nile test catchment.
Lead Author	DCER
Contributors	ECMWF
Distribution	<Please select one of three below> PP: Restricted to other programme participants (including the Commission Services) RE: Restricted to a group specified by the consortium (including the Commission Services) CO: Confidential, only for members of the consortium (including the Commission Services)
Reference	WP4-D4.4

DOCUMENT HISTORY

Date	Revision	Prepared by	Organisation	Approved by	Notes
26/10/2012		Modathir A. H. Zaroug	DCER		
29/10/2012	Elfatih Eltahir		DCER		
12/11/2012		E. Dutra, F. Pappenberger and F. Wetterhall	ECMWF		

ACKNOWLEDGEMENT

The research leading to these results has received funding from the European Union's Seventh Framework Programme (FP7/2007-2013) under grant agreement N°265454

Page intentionally left blank

Summary

The Blue Nile originates from Lake Tana in the Ethiopian Highland and contributes with around 67% of the discharge in the main Nile river. Egypt and Sudan are dependent on the rainfall in the upper catchment of the Blue Nile. Droughts in this region affect agriculture downstream.

In this report we study the impact of sea surface temperature in the Pacific Ocean (Nino 3.4 region) on droughts in the upper catchment of the Blue Nile. The value of several datasets to identify correlations in order to predict droughts and floods in the region is evaluated. This is combined with an evaluation of the discharge measurements (1965-2011) at the outlet of the upper catchment of the Blue Nile in relation to the Nino 3.4 index as well as the effect of start and end of El Nino on droughts of the upper catchment of the Blue Nile. The effect of the start and end of La Nina on floods is also explored. The study demonstrates that a start of an El Nino in April-June is linked to a drought occurrence of 83%. When El Nino was followed by La Nina, there is a 50% chance there will be a record-breaking flood.

Previous DEWFORA WP4 reports identified a reduced agreement between the standard precipitation index calculated using ECMWF ERA-Interim reanalysis and a dataset based on observations in the Blue Nile region. This was associated with an artificial trend of ECMWF ERA-Interim reanalysis precipitation in the region. The present results show that the standard precipitation index calculated with GPCP has a reasonable agreement with remote sensed Normalized Difference Vegetation Index, i.e. dry/wet seasons are associated with positive/negative anomalies in vegetation, while such signal is not found in the ECMWF ERA-Interim reanalysis standard precipitation index. Further evaluation of the potential of using the ECMWF ERA-Interim reanalysis precipitation to monitor meteorological droughts (and associated impacts on vegetation, river discharge, etc…) is limited by the lack of local precipitation observations. The previous results WP4 reports and the new results this report, indicate that the use of the ECMWF ERA-Interim reanalysis for monitoring meteorological drought in the Blue Nile region is restricted and its use should be taken with caution. However, to our knowledge, no other dataset of precipitation, with a better quality, is freely available on near-real time.

Page intentionally left blank

TABLE OF CONTENTS

List of figures

LIST of tables

1. INTRODUCTION

The Nile is the longest river in the world with a length of 6,650 km and it flows through ten countries Jury, (2004). The major two tributaries are the White Nile and Blue Nile. The Blue Nile originates from Lake Tana in Ethiopian Highland and contributes with around 67% to the main Nile discharge. The rainfall regime depends on the seasonal fluctuation of the ITCZ, and the rainy season extends approximately from June to September. The Blue Nile and its tributaries rise on the Ethiopian plateau, at elevations of 2000-3000 m, with several peaks up to 4000 m or more. The two main tributaries are Rahad and Dinder. The Blue Nile sustains the life of millions of people in Ethiopia, Sudan and Egypt.

Rainfall has a great effect on the social and economic life in the region. Scarcity in rainfall leads to drought while excessive, intense rainfall may lead to floods. For example, in the 1984 drought in Sudan, Khartoum received only 4.7 mm of rain between May and October Eltayeb (2003). This led to crop failure and consequently a famine hit Sudan which in turn led to people migrating in search of food and water. Floods reflect the other extreme in rainfall fluctuations. There are many factors which affects the severity of the flood, such as terrain slopes, soil types and amount of water in the soil. On the 4th of August 1988, Khartoum received 216 mm of rainfall during a 24 hour-period. This situation became disastrous when the Nile rose around 7m above normal, which led to wide-spread property damages in Khartoum. These two extreme natural disasters were associated with anomalies in the Pacific sea surface temperature (SST): El Nino and La Nina events.

During the last few decades, there has been a wide recognition that natural oscillations in the state of the Pacific Ocean leave a significant impact on the patterns of weather and climate around the world. The dominant among these oscillations is known as the El Nino – Southern Oscillation (ENSO) which has a period of about 4 years. Eltahir, (1996) found that 25% of the natural variability in the annual flow of the Nile is associated with El-Nino oscillations and proposed to use this observed correlation to improve the predictability of the Nile floods. Wang and Eltahir, (1999) recommended an empirical methodology for medium and long-range (~6 months) forecasting of the Nile floods using ENSO information. In this study, we evaluate the hypothesis whether a similar connection can be made for droughts by using a physically based model of the climate system (the Regional Climate Model (RegCM4.1.1)) Giorgi et al., (2012).

This analysis is complemented by an integrated monitoring and forecasting system based on the standardized precipitation index (SPI, Mckee et al. 1993), which is used to classify droughts and was developed and verified for different African regions in the DEWFORA

D4.3 (2012) (hereafter D4.3). A full evaluation of the SPI monitoring and forecasting skill was conditioned on the available precipitation observations. To extend this verification, we compared the evolution of the SPI at different time scales with the normalized difference vegetation index (NDVI) in the Blue Nile region. The NDVI is computed as the difference (in reflectance) between the near-infrared and visible bands divided by the sum of these two bands (Sellers 1985). The use of visible/near infrared vegetation indices is a common practice in monitoring agricultural drought (both extension and severity) (e.g. Kogan 1995). The SPI at different accumulation time-scales reflect soil moisture deficits that will influence vegetation. However, vegetation is not only controlled by precipitation/soil moisture availability, other factors such as available solar radiation, temperature and irrigation will impact the vegetation development. Therefore, in the present analysis, we will focus on the identification of SPI time-scales and seasons where there is a clear relation with NDVI, and verify if those relations are present in the drought monitoring dataset developed in D4.3. The first part of this report will present the datasets and methods used. This is followed by results and conclusions.

2. DATA AND METHODS

2.1 OBSERVED DATA

Discharge measurements between 1965 and 2011 from the Eldiem station (Figure 2.1) located at the border between Sudan and Ethiopia around 120 km upstream the El Rosieres dam (Figure 2.1) was used in this study. The gauge station measures water level and discharge at the outlet of the upper catchment of the Blue Nile. The data at Eldiem station from 1997 to 2001 was missing. These missing data were substituted by the nearest station (Rosieres dam station), which is almost similar to Eldiem station.

Amarasekera et al., (1997) showed that ENSO episodes are negatively correlated with the floods of the Blue Nile and Atbara rivers that originate (rivers) in Ethiopia. Eltahir, (1996) showed that the probability of having a low (high) flood given a cold SST condition is 2% (49%). On the other hand, the probability of having a high (low) flood given a warm SST condition is 8% (58%). In this study we use an ensemble of 9 average members to study the impact of Nino 3.4 on the drought and flood in the upper catchment of the Blue Nile.

For the El Nino, the Nino 3.4 index between 1965 and 2011 was downloaded from NOAA. Nino 3.4 is defined as 5 consecutive three-month averages of sea surface temperature above +0.4 relative the climatic mean calculated from 1950-1979 for a region of the equatorial Pacific (Niño 3.4 region; 120W-170W, 5N-5S).

Niño 3.4 region was correlated with the observational datasets: GPCP (2.5°×2.5° resolution; Adler et al.2003). GPCP is a satellite gauge-merged rainfall product.

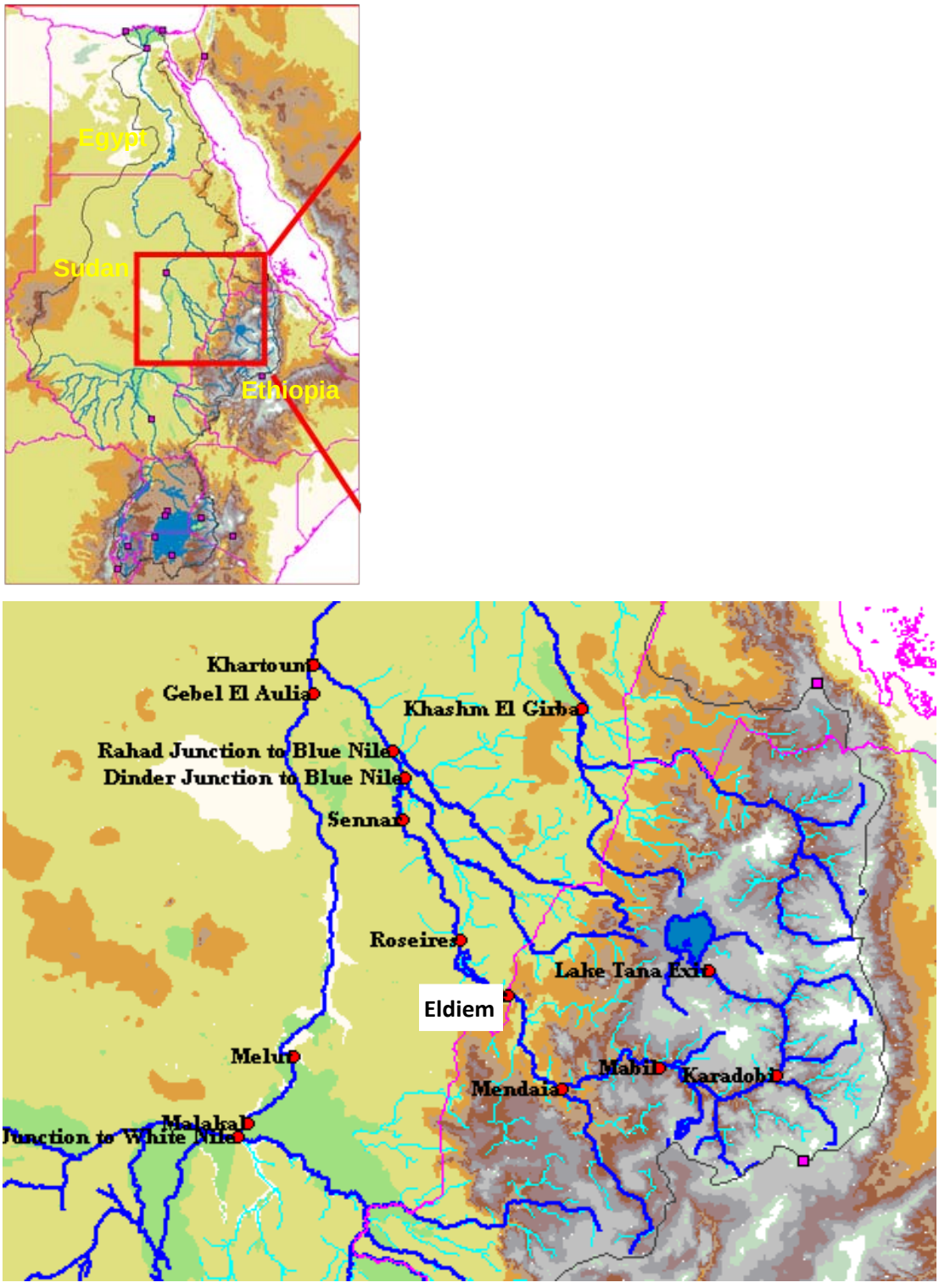

Figure 2.1: The topography and names of the cities in the region.

Two global datasets of monthly precipitation, previously used in DEWFORA D4.3, were selected. The ECMWF ERA-Interim reanalysis available from January 1979 onwards to near-real time with an horizontal resolution of about 80 km and the Global Precipitation

Climatology Project (GPCP) version 2.2 (Huffman et al. 2011) available from January 1979 to December 2010 with a resolution of 2.5°. Further details of these datasets and of the SPI calculations can be found in D4.3. In D4.3, ERA-Interim was proposed to be used for monitoring of meteorological drought (because of its near-real time update), whereas GPCP was used for verification.

In this report, we have used the Global Inventory Modelling and Mapping Studies (GIMMS) NDVI dataset (Pinzon et al. 2005; Tucker et al. 2004; Tucker et al. 2005). This dataset is available for June 1981 to December 2006 with a monthly temporal resolution and 8 km spatial resolution. Ji and Peters (2003) compared this NDVI product with SPI over U.S. Great Plains and found the highest correlations during the middle of the growing season (June to September), and lower correlations at the beginning and end of the growing seasons.

2.2 REGCM4 MODEL DESCRIPTION

RegCM4 is an evolution of the previous version, RegCM3, described by Pal et al., (2007). RegCM4 is a hydrostatic, sigma-p vertical coordinate model with multiple physics options. For this experiment we used the options described in Giorgi et al., (2012): modified CCM3 radiative transfer scheme Kiehl et al., (1996), modified Holtslag et al., (1990) planetary boundary layer scheme, SUBEX resolvable precipitation scheme Pal et al., (2000), mixed cumulus convection configuration utilizing the scheme of Grell, (1993) over land and that of Emanuel, (1991) over oceans and the biosphere−atmosphere transfer scheme Dickinson et al., (1993) land surface package. The horizontal resolution of the model is 125 km. In a north−south direction the domain extends from about 50° S to 50° N, and a standard exponential relaxation procedure Giorgi et al., (1993a) are used in the southern and northern boundaries over a buffer zone with 12 grid points width. Therefore, the model uses forcing lateral BC only in the northern and southern boundaries of the domain, with no external forcing in an east−west direction. The model has 18 vertical sigma levels and a top at 50 hPa, as in its standard configuration.

The initial and lateral boundary conditions for the RegCM4.1 simulations were obtained from the ERA-Interim 1.5° × 1.5° gridded reanalysis (ERAI, Dee et al. 2011) which is the third generation ECMWF reanalysis products. RegCM4.1 was forced with sea surface temperatures (SSTs) obtained from the National Oceanic and Atmospheric Administration (NOAA) Optimum Interpolation (OI) SST dataset (Reynolds et al., (2007).

The simulation period was from 1 January 1982 to 31 March 2010. The observed data used for model validation was the Global Precipitation Climatology Project daily precipitation dataset (GPCP, 1° × 1° resolution; Huffman et al., (2001).

3. RESULTS AND DISCUSSION

3.1 EL NINO AND LA NINA YEARS AND THEIR EFFECT IN THE DISCHARGE OF THE UPPER CATCHMENT OF THE BLUE NILE.

The discharge at El diem station and its association with El Nino and La Nina years is shown in Fig. 3.1. El Nino years like 1972 and 1987 are associated with low discharge, and La Nina years, for example 1988 with high discharge.

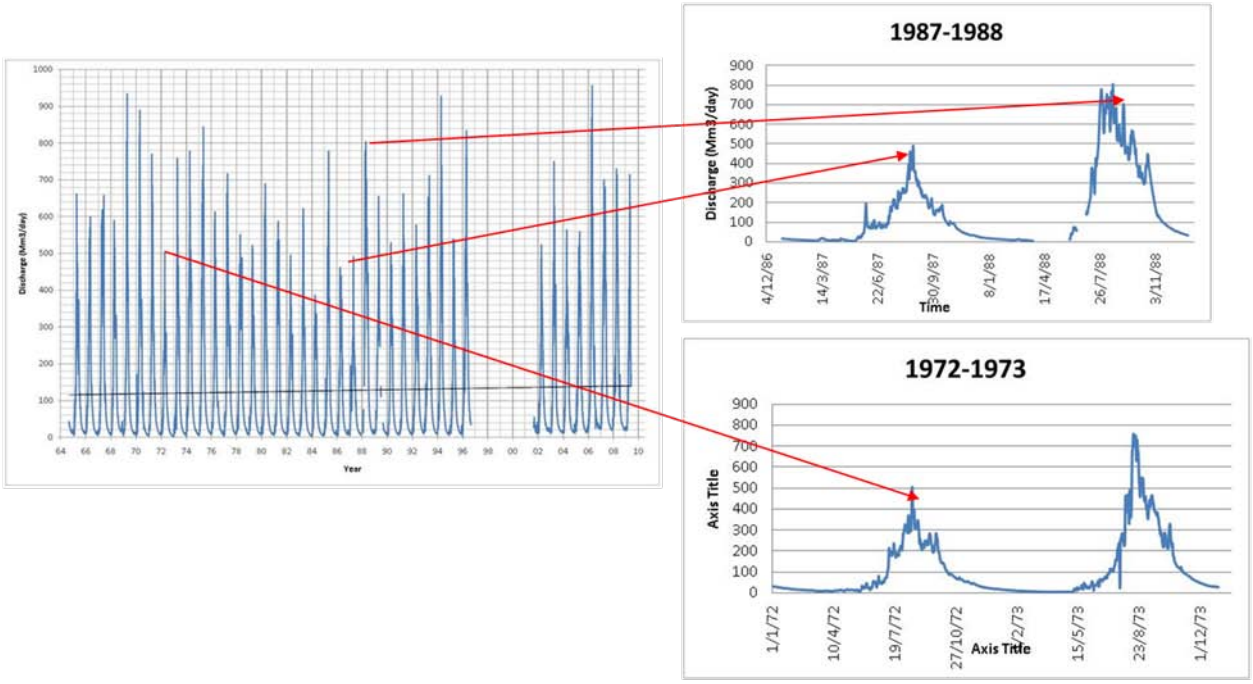

Figure 3.1: The discharge of the Blue Nile at El diem station (1965-2011) and its association with El Nino and La Nina years

3.2 TELECONNECTIONS OF PACIFIC SST AND THE DISCHARGE OBSERVATION AT EDIEM STATION.

The seasonal discharge anomalies for JJAS are shown in Figure 3.2. Some thresholds were assumed in this study: any discharge anomaly above 9500×10^6 m^3 was considered as high flood, and any discharge anomaly below -9500×10^6 m^3 considered as a severe drought, and any discharge between 38250×10^6 m^3 and 9500×10^6 m^3 considered as flood, and any discharge between -3825×10^6 m^3 and -9500×10^6 m^3 considered as a drought. Finally, any discharge between -3825×10^6 m^3 and 3825×10^6 m^3 was considered normal. This classification is in line with observed floods and droughts in this region. For example, in Figure 3.2 7 high floods can be identified, and among them there three extremely high floods in 1988, 2006 and 2007. There are 5 extreme droughts, 6 normal floods, and 11 droughts.

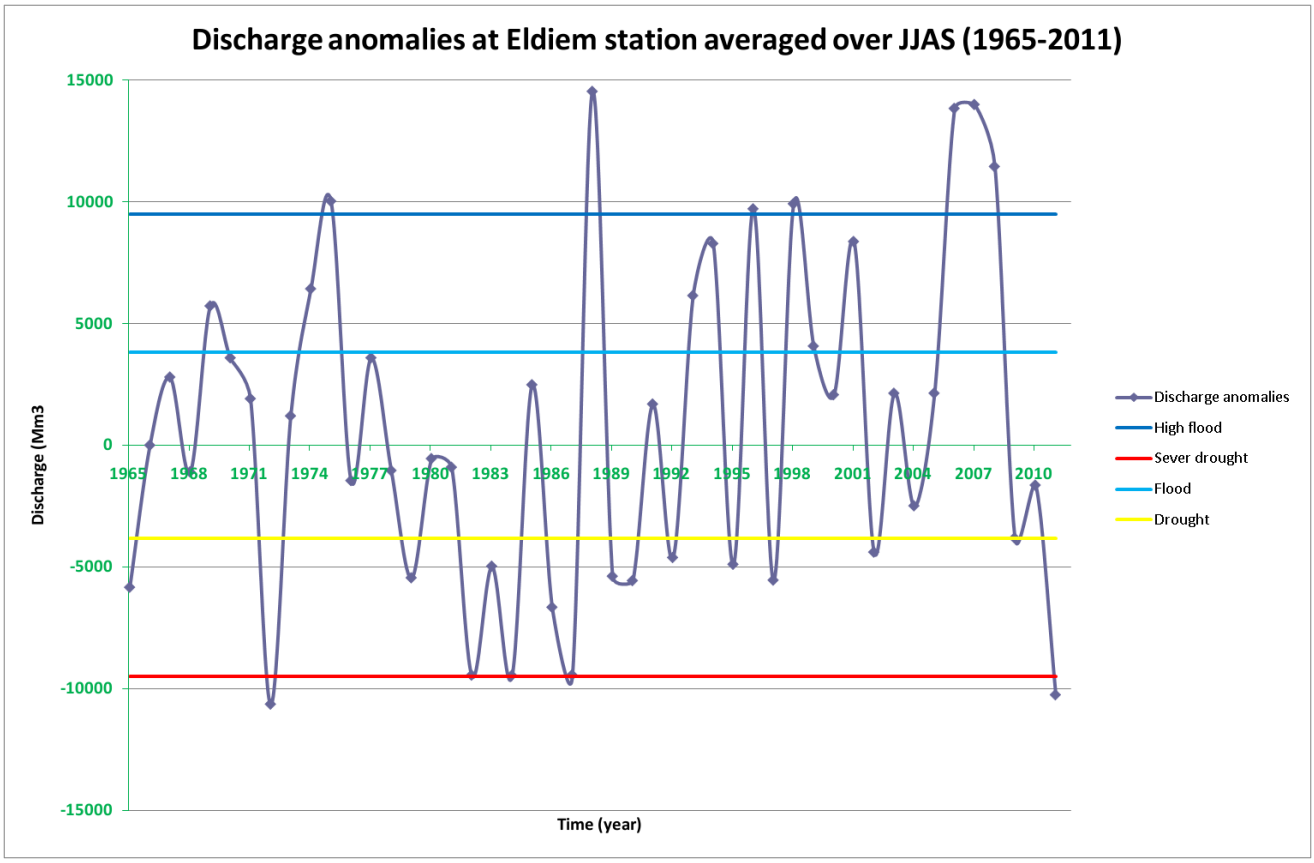

Figure 3.2: The discharge anomalies at Eldiem station averaged over JJAS (1965-2011), the dark blue line represent the threshold for the high flood, and the light blue line represents the threshold for normal flood, and the yellow line represents the threshold for the normal drought and the red line represents the severe drought.

3.2.1 The effect of start of El Nino.

The effect of start of El Nino in the drought of the upper catchment of the Blue Nile was investigated by evaluating the relationship between Nino 3.4 for different seasons, and the rainfall anomaly in the upper catchment of the Blue Nile during June to September (JJAS) for each year respectively. The first column in Table 3.1 shows the starting season of El Nino, the second column indicates whether there was a strong drought, the third column if there was a normal drought, and the fourth column if there is no drought in the upper catchment of the Blue Nile. The year column refers the start year of each El Nino event. The length column refers to the number of months during that El Nino.

Table 3.1: The effect of the start of El Nino in the drought of the upper catchment of the Blue Nile during JJAS of the same year.

Start of El Nino	Strong drought	Drought	No drought	Year	Length
AMJ	✓			1972	11
AMJ	✓			1982	14
AMJ		✓		1965	12
AMJ		✓		1997	12
AMJ		✓		2002	10
AMJ			✓	1991	14
JJA			✓	2004	7
JJA		✓		2009	10
JAS			✓	1968	18
			✓	1969	
JAS		✓		1986	19
	✓			1987	
ASO			✓	1976	6
ASO			✓	1977	6
ASO			✓	1994	7
ASO			✓	2006	5

From Table 3.1 there are six events when El Nino started in AMJ. When El Nino started in AMJ, there was a strong drought twice, 3 droughts and only one year with normal conditions.. When El Nino started in JJA, there was only 1 drought. The longest two El Nino events occurred when El Nino started in JAS. When El Nino started in JAS there was no drought on the same year, but the discharge was below average, and there was one drought event. When El Nino extends to the whole next year, there was one strong drought (in 1987), and one normal year (in 1969). When El Nino started late in ASO there was no drought event (in the same year) for four times, among them one normal flood and one high flood.

From the above results and Table 3.1, we found that the upper catchment of the Blue Nile is very sensitive to El Nino events starting in AMJ. When El Nino started in AMJ, 5 out of 6 cases there was a drought. When El Nino started in JJA or JAS, 50% of the cases there was a drought. If we look at these three seasons in total (AMJ, JJA and JAS), in 70% of the cases, there was a drought in the upper catchment of the Blue Nile, in 20% of the cases the discharge was below average, and only in 10 % of the cases no drought was observed. When El Nino starts late (ASO), there are no drought effects in the Blue Nile.

3.2.2 The effect of the end of El Nino

Similar to the previous analysis, we compared the relation of the end of El Nino with drought occurrence in the upper catchment of the Blue Nile. The first column in Table 3.2 shows the season of the end of El Nino.

Table 3.2: The effect of the end of El Nino in the drought of the upper catchment of the Blue Nile during JJAS of the same year.

End of El Nino	Strong drought	Drought	No drought	Year	Length
DJF			✓	1970	18
DJF			✓	2005	7
DJF			✓	2007	5
JFM			✓	1977	12
JFM			✓	1978	12
JFM			✓	1988	10
JFM			✓	2003	10
FMA			✓	1973	11
FMA		✓		1995	7
MAM			✓	1966	12
MAM			✓	1988	12
MAM			✓	2010	10
MJJ		✓		1983	14
MJJ		✓		1992	14

When El Nino ended early in DJF or JFM, there was no drought in the same year during JJAS. When El Nino ended in FMA, there was one drought event (in the same year). When El Nino ended in MAM, three times there was no drought in the same year. However, when El Nino ended in MJJ, two times there was a drought (in the same year).

The previous analysis indicates that when El Nino ends early (DJF, JFM, FMA and MAM) there is almost no impact on drought occurrence in the upper catchment of the Blue Nile. When El Nino ended late in MJJ (or after that) there is a high possibility of having drought in the upper catchment of the Blue Nile.

3.2.3 The effect of start of La Nina.

La Nina is normally associated with floods in the upper catchment of the Blue Nile. In this section the start of La Nina season will be explored, along with its effect on the flooding of the upper catchment of the Blue Nile in the same year. The first column in Table 3.3 shows the season of the start of La Nina. From Table 3.3, it is clear that La Nina events can last for three years, as in 1973-1975 and 1998-2000.

When La Nina started in AMJ, there was one strong flood, one flood and one year with normal conditions (in the same year). Similar event frequencies were found when La Nina started in JJA. When La Nina started late in ASO, there were no floods recorded, and in one event there was a strong drought. When La Nina extended for the next year, years or at least

9 months of the next year, there were no floods for three times (all of them above average), two times there was a flood, and one time a high flood.

Table 3.3: The effect of the start of La Nina in the flood of the upper catchment of the Blue Nile.

Start of La Nina	Strong flood	Flood	No flood	Year	Length
AMJ			✓	1973	36
		✓		1974	
	✓			1975	
AMJ	✓			1988	13
JJA		✓		1970	18
			✓	1971	
JJA	✓			1998	33
		✓		1999	
			✓	2000	
JJA			✓	2010	10
JAS	✓			2007	11
	✓			2008	
ASO			✓	1983	5
ASO			✓	1995	7
ASO			✓	2011	7

3.2.4 The effect of the end of La Nina.

When La Nina Ended in DJF (see Table 3.4), three times there was no flood in the upper catchment of the Blue Nile. When La Nina ended in FMA, there were two times a strong flood (in the same year), and one time a flood. When La Nina ended in MAM, there were no floods twice. When La Nina ended in AMJ, there was no flood (in the same year). When La Nina ended in MJJ or ASO, there was no flood (in the same year).

Table 3.4: The effect of the end of La Nina in the flood of the upper catchment of the Blue Nile.

End of La Nina	Strong flood	Flood	No flood	Year	Length
DJF			✓	1965	9
DJF			✓	1972	19
DJF			✓	1984	5
FMA	✓			1996	7
FMA		✓		2001	33
FMA	✓			2006	5
FMA				2012	7
MAM			✓	1976	36
MAM			✓	2011	10
AMJ			✓	1989	13
MJJ	✓			2008	11
ASO			✓	1985	12

3.2.5 El Nino followed by La Nina and the breaking record flood.

In the last 40 years when El Nino was followed by La Nina there were high floods records in the upper catchment of the Blue Nile in 1988, 1998 and 2007. When El Nino was followed by La Nina, in 50 % of the cases there were breaking record floods as shown in Table 3.5. The red box represents the end of El Nino period, and the blue box represents the start of La Nina.

Table 3.5: El Nino followed by La Nina and high flood.

Year	DJF	JFM	FMA	MAM	AMJ	MJJ	JJA	JAS	ASO	SON	OND	NDJ	Remark
1970	-						+						Low flood
1973			-		+								Above average
1988		-			+								**High flood**
1998				-			+						**High flood**
2007	-							+					**High flood**
2010				-			+						Below average

3.3 THE CORRELATION BETWEEN NINO 3.4 AND THE GPCP PRECIPITATION OBSERVATIONS.

In the previous sections we evaluated the relations between Nino 3.4 and discharge at the upper catchment of the Blue Nile. Figure 3.3 shows the rainfall anomalies over the upper catchment of the Blue Nile during JJAS from 1982 to 2011. GPCP does not capture all the years as shown in Figure 3.2. GPCP underestimated the rainfall in 1987, and did not capture the floods in 2007 and 2008, while overestimating the rainfall in 2009 and 2010.

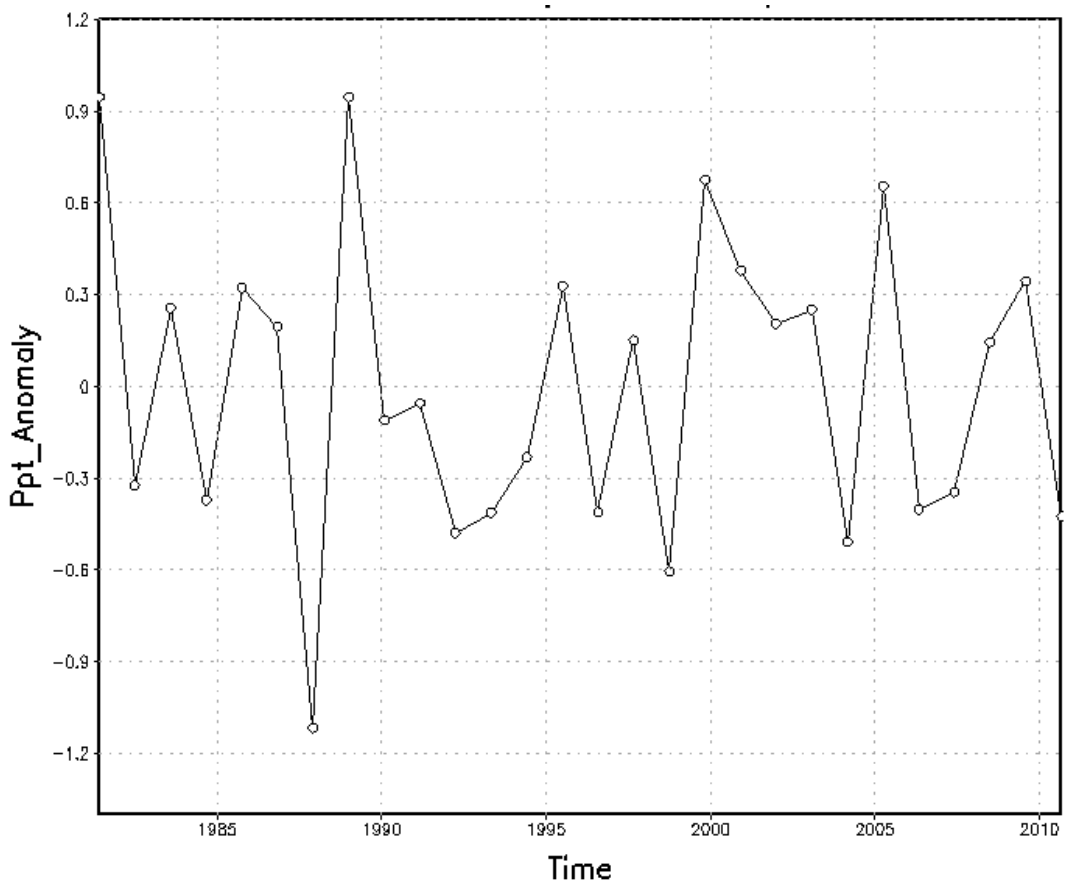

Figure 3.3: Rainfall anomalies over Ethiopian Highlands during JJAS.

The correlation between the SST anomalies in Nino 3.4 region during different seasons was calculated against the rainfall over Ethiopian Highland from the GPCP as shown in Table 3.6. The negative and lowest correlations were found during JFM season, the negative correlation increased gradually until JJA (-0.64).

Table 3.6: The correlation between SST anomalies in Nino 3.4 region and the upper catchment of the Blue Nile in Ethiopian Highlands

SST anomalies	Rainfall over Ethiopian Highland from GPCP	Correlation
JFM	JJAS	-0.02
FMA	JJAS	-0.10
MAM	JJAS	-0.26
AMJ	JJAS	-0.48
MJJ	JJAS	-0.63
JJA	JJAS	-0.64

3.4 MODEL RESULT ANALYSIS.

Figure 3.4 shows the model domain and topography along with some sub-regions selected for more detailed regional analysis.

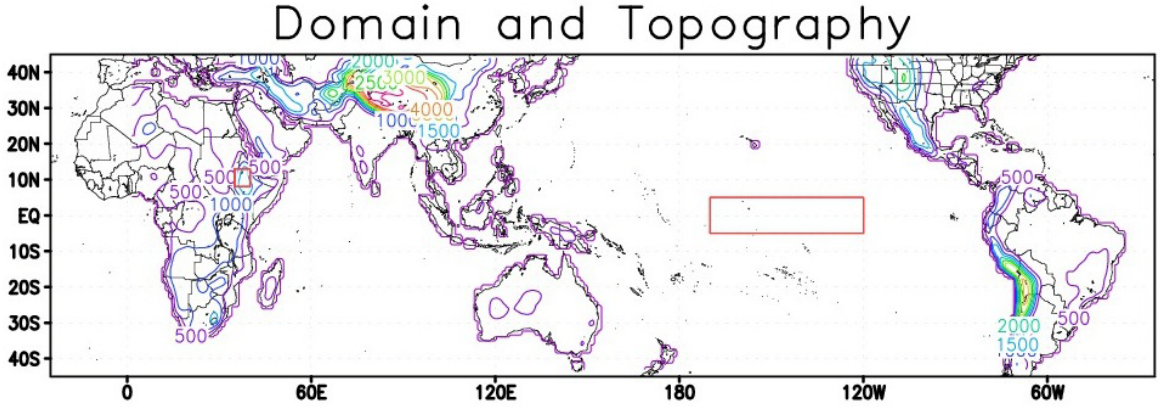

Figure 3.4: The domain and the topography of the model. The red box in the Pacific Ocean illustrated Nino 3.4 region, and the red box in Ethiopian Highland illustrated the upper catchment of the Blue Nile.

3.4.1 The difference between La Nina and El Nino years in the model and in the observational data set.

In this analysis we assess if the model (RegCM4.1) was able to capture the difference between La Nina and El Nino years. The 9 members were averaged for 28 years (1982-2009), and then 5 La Nina years and 5 El Nino years were selected. In the upper panel of Figure 3.5, the average of 5 La Nina years (1988, 1998, 1999, 2007 and 2008) are shown, and

in the middle panel the average of 5 El Nino years (1982, 1983, 1987, 1992 and 2002). The lower panel shows the difference between the La Nina years and the El Nino years, with rainfall differences in the Sahel region and in the upper catchment of the Blue Nile. The results of each ensemble member are shown in Figure 6.1 to Figure 6.9. These model results agree with the previous analysis, confirming that La Nina years are associated with the above normal rainfall and El Nino years with below normal rainfall in the upper catchment of the Blue Nile. So, the model can capture the impact of El Nino/ La Nina.

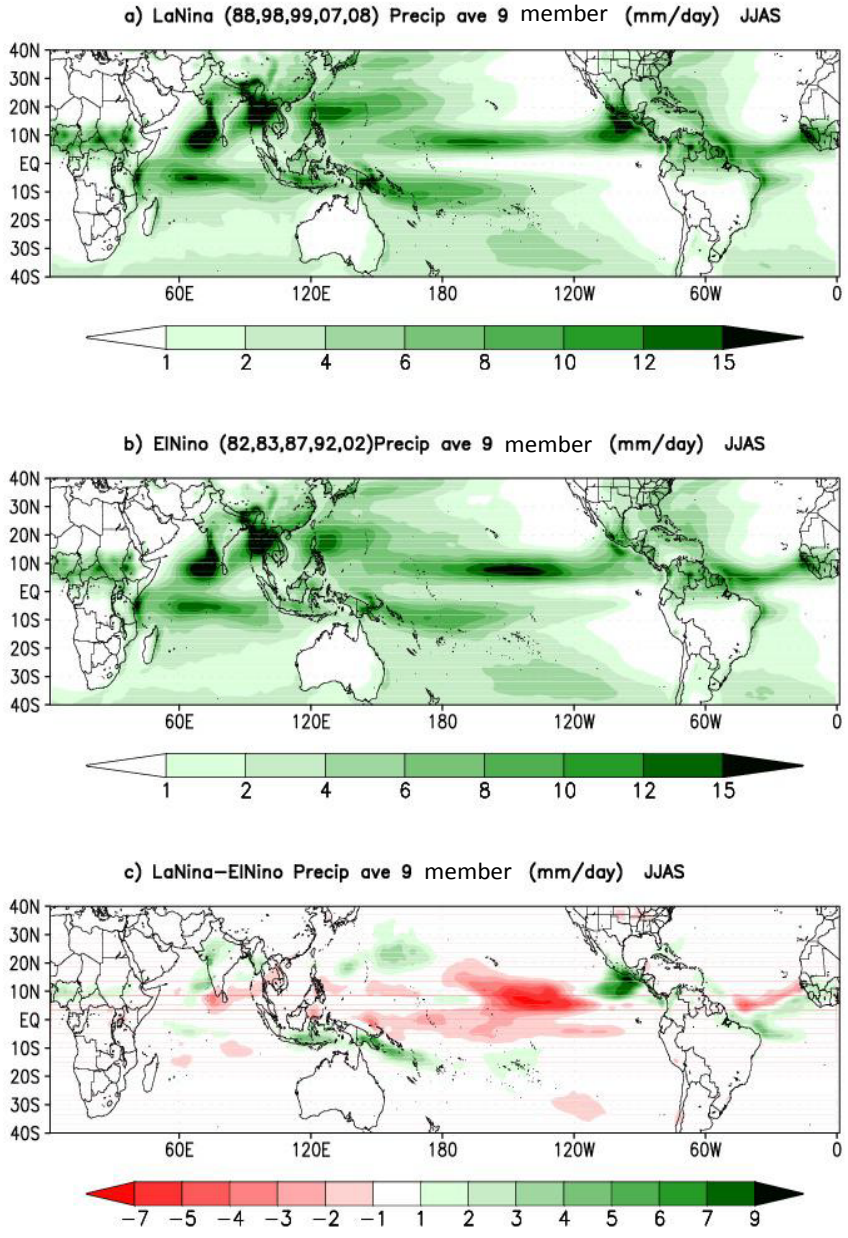

Figure 3.5: The rainfall during JJAS for a) 5 La Nina years b) 5 El Nino years c) The difference between La Nina years and El Nino years.

3.4.2 Correlation between rainfall anomalies over Ethiopian Highlands and SST anomalies over the Pacific Ocean in Nino 3.4 region for 9 members.

Figure 3.6 shows the correlation between the rainfall anomalies during JJAS and the SST anomalies during (JFM, FMA, MAM, AMJ, MJJ and JJA). The correlations are negative during all seasons. The lowest correlation was around 42 % in JFM and it increased gradually up to AMJ. The highest correlation was around 62% during AMJ. After that, the correlations decreased to 49% in JJA. In section 3.2 the river discharge showed the highest probability for drought events during AMJ (83 %). The model results also show the highest correlation during AMJ. These results support the use Nino3.4 in AMJ for a seasonal forecasting of drought in the upper catchment of the Blue Nile.

The previous correlations were calculated for each member, and are represented in the appendix in Figure 6.10 to Figure 6.18. The best correlation was found when taking the ensemble mean.

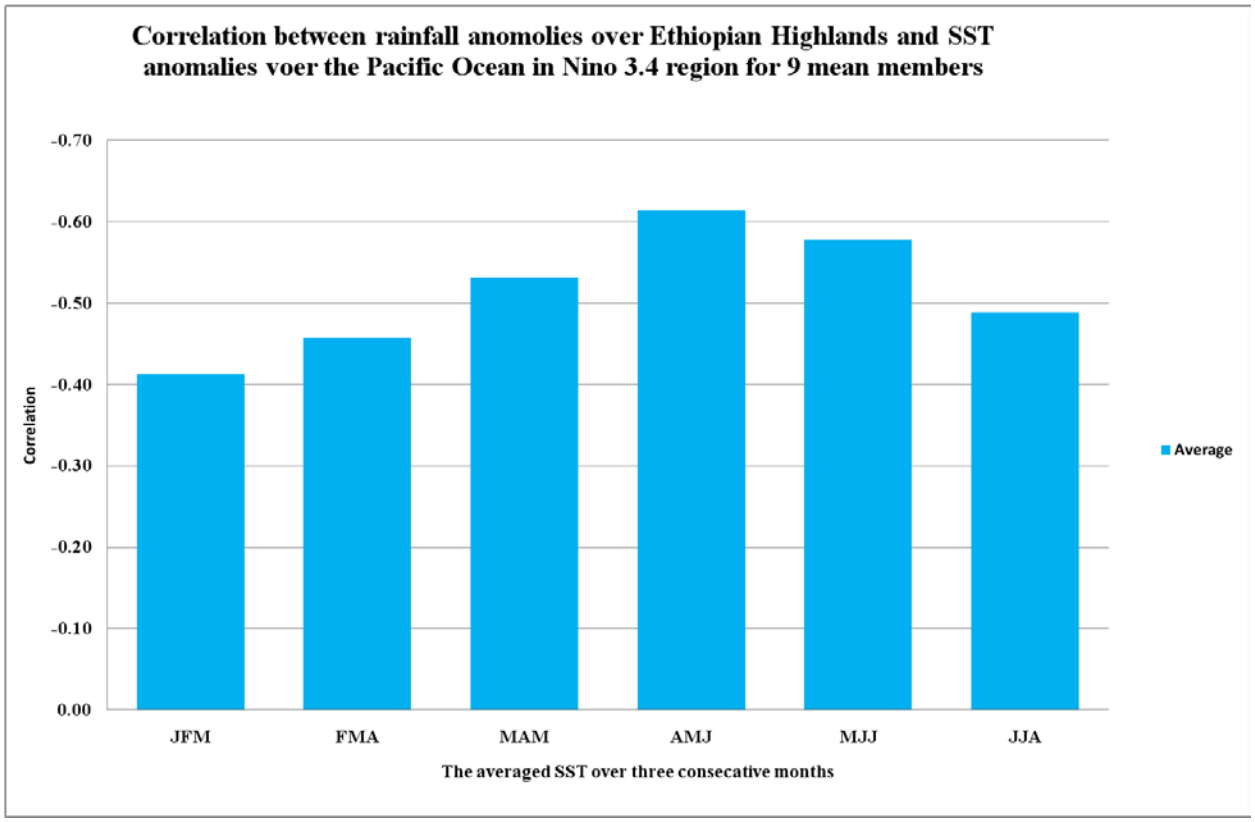

Figure 3.6: The correlation between rainfall anomalies over Ethiopian Highlands for 9 averaged members and SST anomalies over the Pacific Ocean in Nino 3.4 region.

The negative correlation between the SST anomalies in Pacific Ocean in Nino 3.4 region and the rainfall in the upper catchment of the Blue Nile during JJAS is displayed in Figure 3.7. The left axis represents the SST anomalies in different seasons, and the right axis the ensemble mean JJAS rainfall anomaly. Similar analyses for each ensemble member are shown in Figure 6.19 to Figure 6.27.

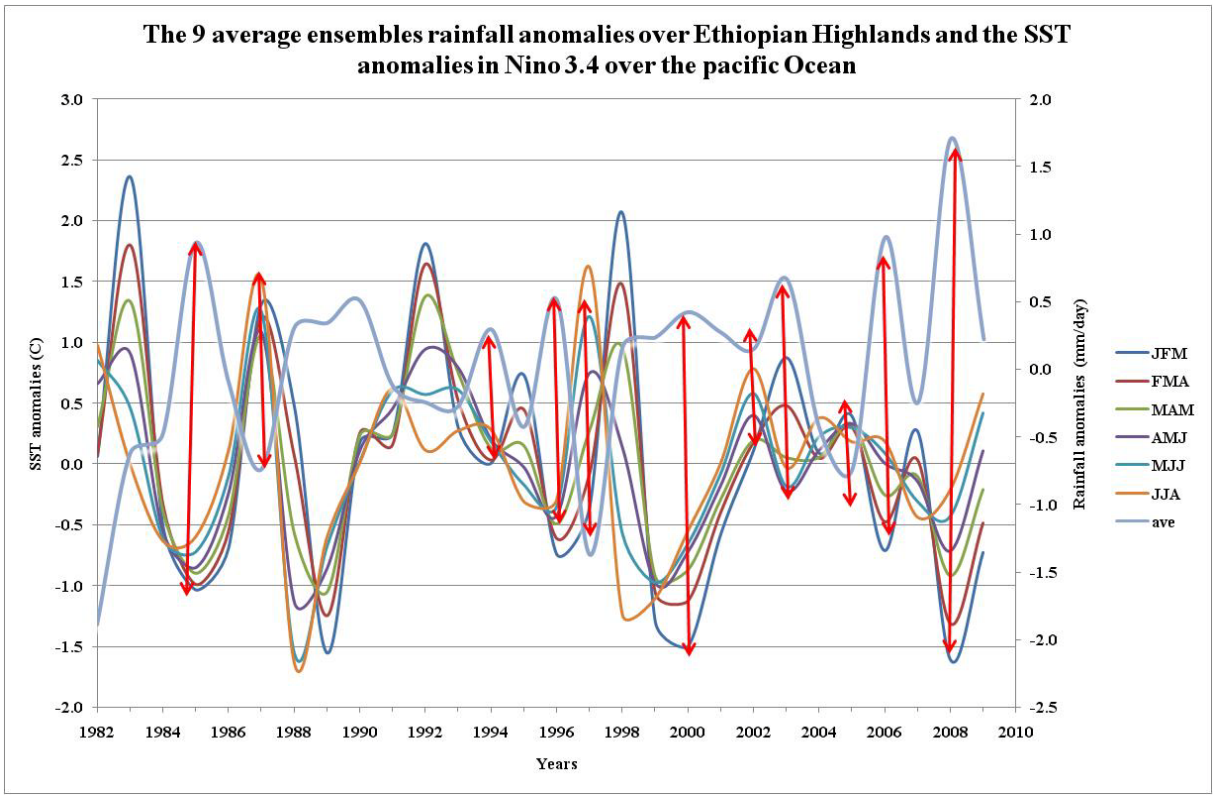

Figure 3.7: The SST anomalies during different seasons in Nino 3.4 region and the rainfall anomalies in the upper catchment of the Blue Nile for 9 averaged members.

3.4.3 Regression analysis of DJF and JJA for Nino 3.4 index onto RegCM rainfall for 9 members (1982 -2009).

In this section we present a regression analysis between Nino 3.4, in different seasons (DJF and JJA), and the GPCP and model rainfall. The upper panel of Figure 3.8 represents the regression of DJF Nino 3.4 index onto DJF GPCP rainfall from 1982 to 2009, while the lower panel of Figure 3.8 shows the regression of JJA Nino 3.4 index onto JJA GPCP. The same analysis was performed on the ensemble mean for the two seasons (DJF and JJA). The model results agree with the observational based regression, showing no effect on the rainfall during the low flow in the upper catchment of the Blue Nile as shown in the top panel of Figure 3.9. The lower panel of Figure 3.9 shows a negative signal of the regression in Ethiopian Highland during JJA (around -1). However the band and the length of the negative regression is small compare to the observational based results.

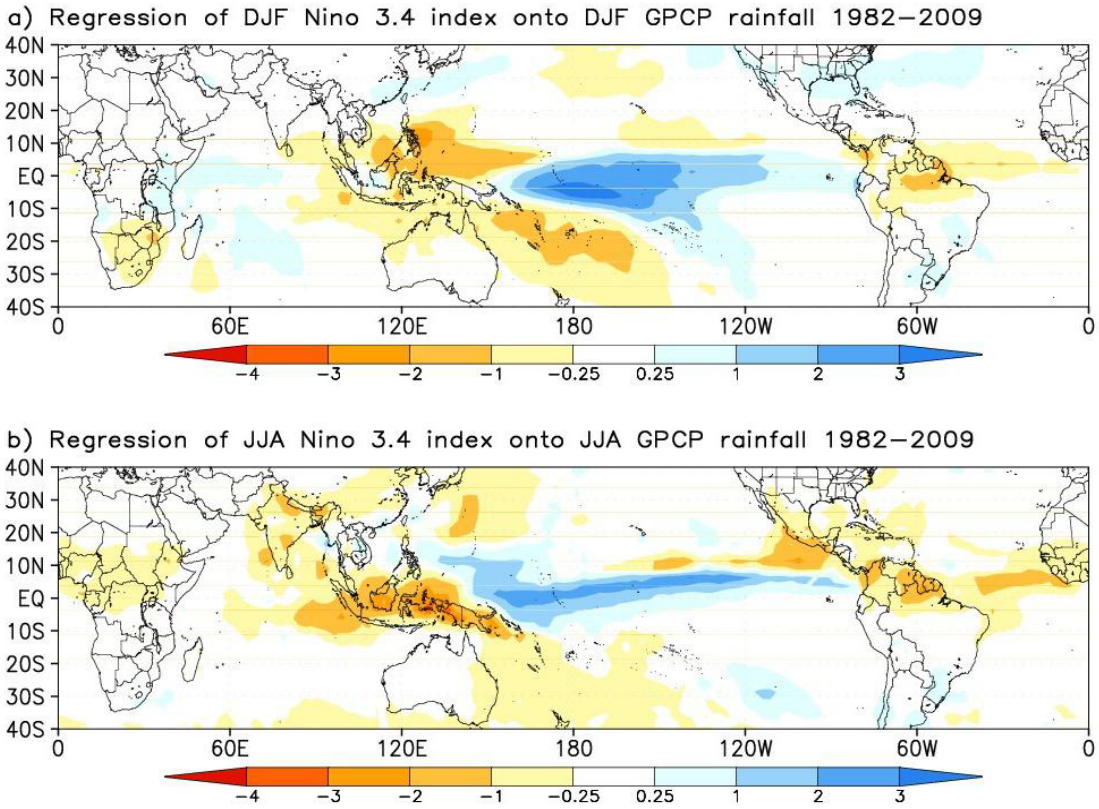

Figure 3.8: Regression of DJF and JJA of Nino 3.4 index onto DJF and JJA for GPCP rainfall for (1982-2009).

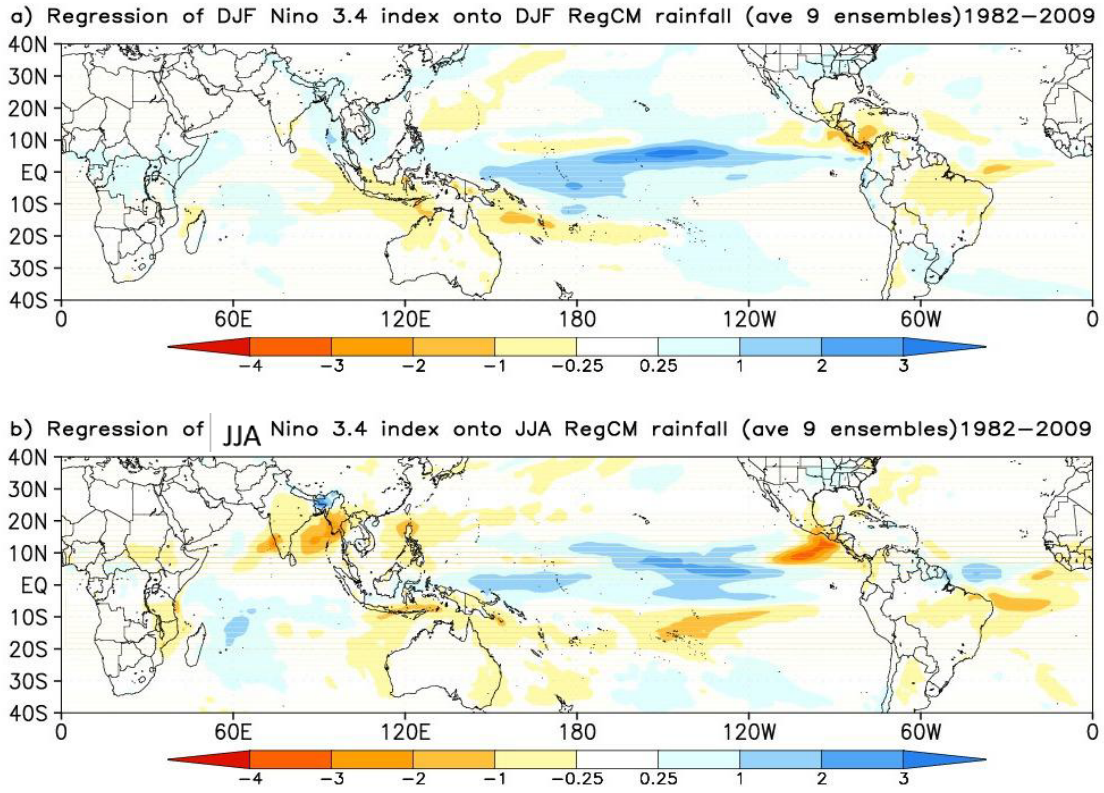

Figure 3.9: Regression of DJF and JJA of Nino 3.4 index onto DJF and JJA rainfall for 9 averaged members for (1982-2009).

3.5 FUTURE ENSO

The El Nino Southern Oscillation (ENSO) phenomenon plays an important role in medium to long range forecast for the Nile River (Wang and Eltahir, (1999)). Monitoring and predicting ENSO can lead to disaster risk reduction through early warning. The orbital variations could affect the ENSO behaviour Jansen et al., (2007) and the 11 year sun cycle can affect ocean temperatures associated with ENSO Meehl et al., (2009). A study found that the long term changes in the behaviour of ENSO might happen without forcing from radiative changes Wittenberg, (2009), wherea another study found that the change of the phenomenon could be stimulated by seasonal changes in solar insolation Cane, (2005). Vecchi and Wittenberg, (2010) found that the variations in ENSO frequency and intensity are due to chaotic behaviour resulting from external radiative forcings. The Nino 3.4 region in the Pacific Ocean (120 W, 170 W, 5 N, 5 S) has trend towards more frequent or stronger El Niño episodes over the past 50 to 100 years (Vecchi and Wittenberg, (2010)). The tendency for recent SST El Niño episodes to be centred in the equatorial Pacific more in the central equatorial Pacific than in the east Pacific Yeh et al., (2009), and increasing in intensity for these central Pacific episodes Lee and McPhaden, (2010). These changes in El Nino episodes may explain the severe

drought in remote areas like Horn of Africa in the recent years. The effect of the greenhouse gases on the behaviour of ENSO over the past 50 to 100 years is uncertain. Yeh et al., (2009) attribute the change of the behaviour of El Niño to the changes in the temperature which, associated with increases in greenhouse gases, whereas Power and Smith, (2007) suggest that changes in the El Nino behaviour is within the range of natural variability.

The IPCC AR4 report mentions that the projected behaviour of the ENSO interannual differs between models; however, all the models exhibited continued ENSO interannual variability in projections through the 21st century Seneviratne et al., (2012).

The current limitation of understanding the ENSO activity leads to lack of confidence to predict whether ENSO activity will be enhanced or damped due to anthropogenic climate change, or even if the frequency of El Niño or La Niña episodes will change Collins et al., (2010). This results in low confidence in projections of changes in the phenomenon. However there is some agreement by most GCMs in projecting increase of the frequency of central equatorial Pacific events (Seneviratne et al., (2012)).

3.6 RELATION BETWEEN THE STANDARDIZED PRECIPITATION INDEX AND REMOTE SENSED VEGETATION

The following analysis will be focused in the Blue Nile (BN) region defined here as: 35°E to 40°E, 8°N to 13°N (see box in Figure 3.10). The mean annual (1981-2006) NDVI in the Nile region is represented in Figure 3.10, along with the mean annual precipitation from GPCP and ERAI. We identify the North-South gradient of NDVI associated to the transition of semi-arid to arid climates, with the exception of the relatively high values of NDVI over the Ethiopian Highlands (BN source is in the North-western region of the Ethiopian Highlands). This signal is also present in ERAI precipitation, while GPCP has only a smooth rainfall peak in the region, due to its lower spatial resolution. The mean annual cycle of precipitation and NDVI averaged over the BN region (see Figure 3.11) shows a significant difference in the precipitation total between GPCP and ERAI, with the latter having much higher values. This had been already identified in D4.3, but without further observations, it is difficult to clearly state that ERAI is overestimating precipitation in the region. The inter-annual variability of ERAI JJAS precipitation in the BN has a poor agreement with observed river discharge (see Figure 3.12), while GPCP partially agrees between wet/dry years and high/low flows.

The NDVI mean annual cycle in the region follows precipitation with a delay of about 1 month. A qualitative evaluation of the mean annual patterns and mean annual cycle of precipitation and NDVI (Figure 3.10 and Figure 3.11) suggests that ERAI has a better

agreement with NDVI than GPCP, mainly due to the spatial definition. However, for drought purposes, we are mainly interested in the intra-seasonal to inter-annual variability.

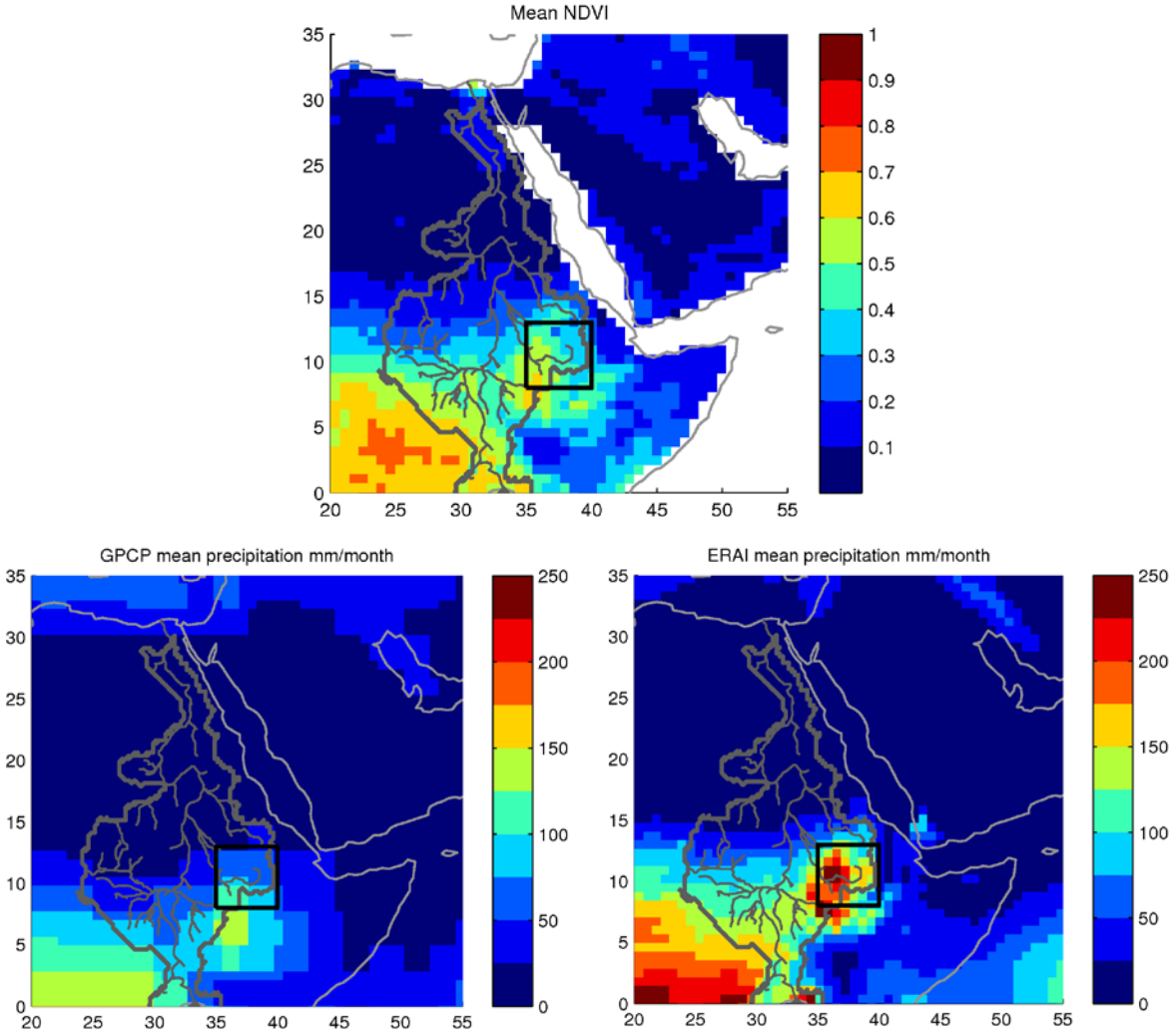

Figure 3.10: Mean annual (1981-2006) NDVI (top panel) and GPCP (bottom left) and ERAI (bottom right) precipitation.

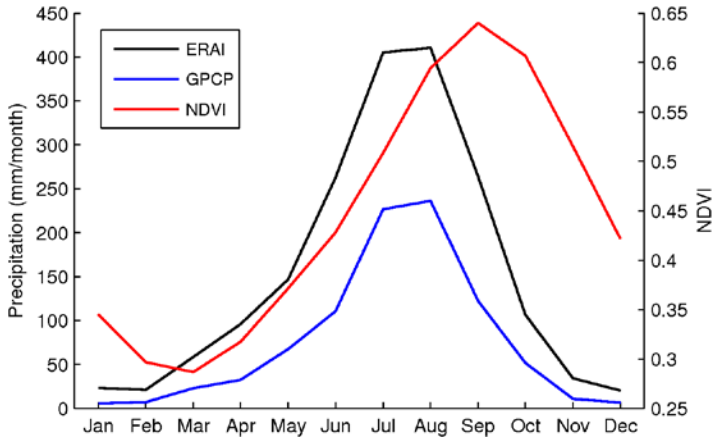

Figure 3.11: Mean annual cycle of ERAI (black) and GPCP (blue) precipitation and NDIV (red) averaged over the Blue Nile (see Figure 3.10) for the period 1981 to 2006.

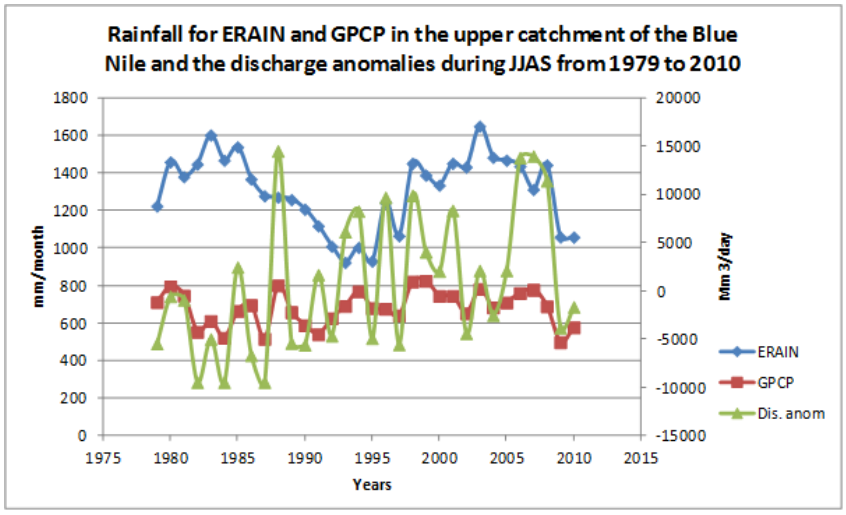

Figure 3.12: Mean JJAS ERA (blue) and GPCP (red) rainfall compared with river discharge anomalies in the upper catchment of the Blue Nile (green).

The agreement between SPI at different time scales and NDVI was evaluated by calculating the grid-point temporal correlation for each calendar month. Figure 3.13 represents the fraction of grid points in the BN region with significant correlations between the GPCP SPI at different time scales and NDVI. Out of the 12 calendar months, May, June, November and December appear as the months with higher fractions of significant correlations associated with the SPI at 3 and 6 months. These correlations indicate a connection between vegetation anomalies and the preceding 3 to 6 months accumulated precipitation anomalies. The low correlations between the SPI and NDVI during the peak rainy season (July-August) indicate that vegetation during that period is not controlled by available soil moisture (since the soils are generally wet).

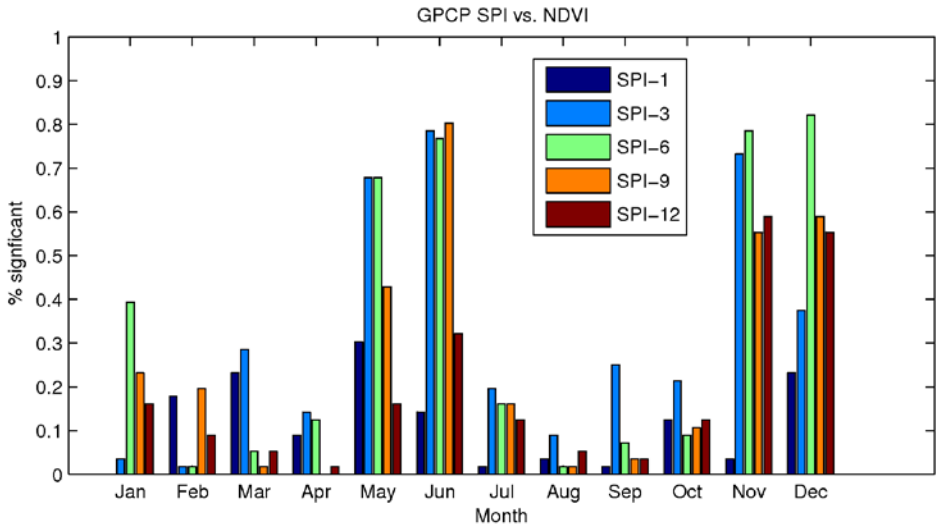

Figure 3.13: Fraction of grid points in the BN region with significant correlation (at 99%) taken for each calendar month between the GPCP SPI at different time scales (different colors) and NDVI.

When a similar diagnostic is applied to the ERAI SPI (Figure 3.14), the fraction of grid points with significant correlations is lower (Figure 3.14).

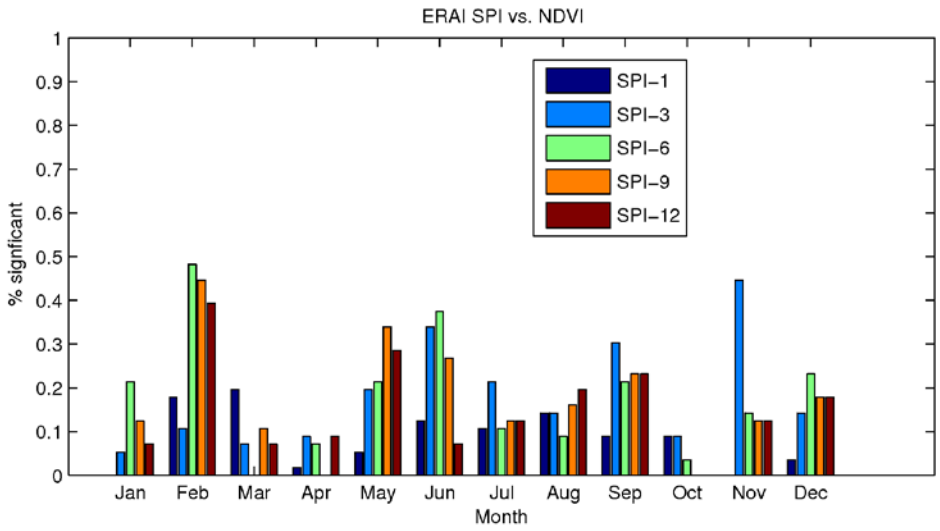

Figure 3.14: As Figure 3.13 but to the ERA-Interim SPI.

The spatial distribution of the maximum correlation between the SPI and NDVI, and the associated SPI time-scale for June is represented in Figure 3.15 for the GPCP SPI and in Figure 3.16 for the ERAI SPI. For the GPCP SPI, there are high correlation values extending

from the Ethiopian Highlands to West, mainly associated with the SPI-3 and SPI-6 (Figure 3.15), while for the ERAI SPI the grid points with significant correlations are very sparse and scattered.

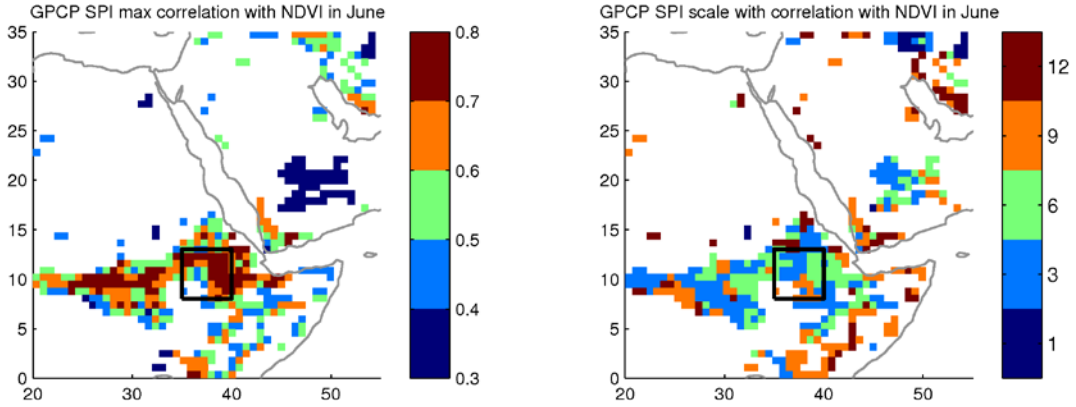

Figure 3.15: Maximum (left) correlation between the GPCP SPI at different time scales and NDVI in June, and the associated SPI time scale with maximum correlation (right).

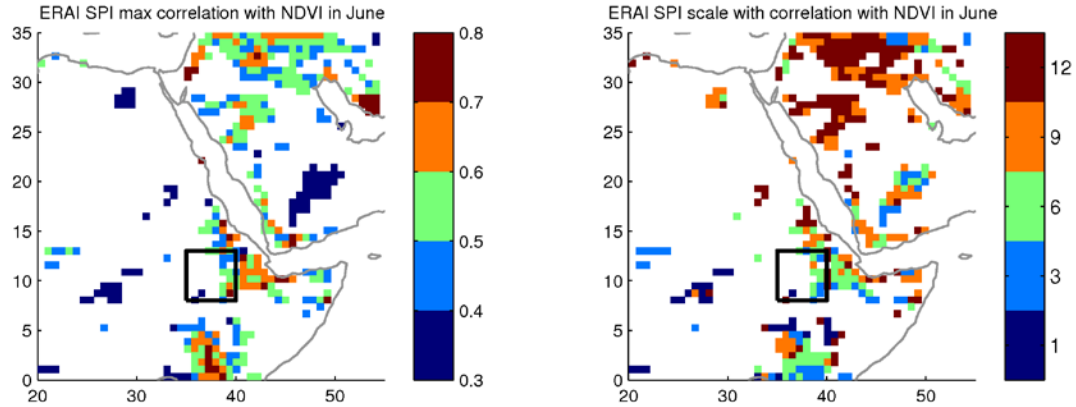

Figure 3.16: As Figure 3.15 but to the ERA-Interim SPI.

4. CONCLUSIONS

Droughts in the Blue Nile are sensitive to El Nino, with 70% of drought cases when El Nino starts in AMJ, JJA and JAS. When El Nino starts in AMJ, 83 % of the cases resulted in drought. When El Nino ends early (DJF, JFM, FMA and MAM), there is almost no effect on the drought in the Blue Nile. When El Nino terminates late in MJJ (or after that) there is a high possibility of drought occurrence in the Blue Nile. When La Nina ended in FMA, there is a high possibility of above normal flows. In 50 % of the cases that El Nino was followed by La Nina there were extremely high flows.

D4.3 identified a reduced agreement between the SPI calculated using ERAI and GPCP in the Blue Nile. This was associated with an artificial trend of ERAI precipitation in the region. The present results show that the GPCP SPI has a reasonable agreement with NDIV, i.e. dry/wet seasons are associated with positive/negative anomalies in vegetation, while such signal is not found in the ERAI SPI. Further evaluation of the potential of using ERAI precipitation to monitor meteorological droughts (and associated impacts on vegetation, river discharge, etc…) is limited by the lack of local precipitation observations. The results of D4.3 and the new results in this report, indicate that the use of ERAI for monitoring meteorological drought in the Blue Nile region is restricted and its use should be taken with caution. However, to our knowledge, no other dataset of precipitation, with a better quality, is freely available on near-real time.

5. REFERENCES

AMARASEKERA, K. N., LEE, R. F., WILLIAMS, E. R. & ELTAHIR, E. A. B. (1997) ENSO and the natural variability in the flow of tropical rivers. *Journal of Hydrology,* 200**,** 24-39.

CANE, M. A. (2005) The evolution of El NiÃ±o, past and future. *Earth and Planetary Science Letters,* 230**,** 227-240.

COLLINS, M., AN, S. I., CAI, W., GANACHAUD, A., GUILYARDI, E., JIN, F. F., JOCHUM, M., LENGAIGNE, M., POWER, S. & TIMMERMANN, A. (2010) The impact of global warming on the tropical Pacific Ocean and El NiÃ±o. *Nature Geoscience,* 3**,** 391-397.

Dee, D. P., S. M. Uppala, A. J. Simmons, P. Berrisford, P. Poli, S. Kobayashi, U. Andrae, M. A. Balmaseda, G. Balsamo, P. Bauer, P. Bechtold, A. C. M. Beljaars, L. van de Berg, J. Bidlot, N. Bormann, C. Delsol, R. Dragani, M. Fuentes, A. J. Geer, L. Haimberger, S. B. Healy, H. Hersbach, E. V. Hólm, L. Isaksen, P. Kållberg, M. Köhler, M. Matricardi, A. P. McNally, B. M. Monge-Sanz, J. J. Morcrette, B. K. Park, C. Peubey, P. de Rosnay, C. Tavolato, J. N. Thépaut, and F. Vitart, 2011: The ERA-Interim reanalysis: configuration and performance of the data assimilation system, *Quart. J. Roy. Meteor. Soc.*, **137**(656), 553-597, doi: 10.1002/qj.828.

DEWFORA D4.3, 2012: Potential to supplementing drought early warning systems with new meteorological information. DEWFORA deliverable D4.3. Available online: http://www.dewfora.net/Publications.

DICKINSON, R. E., HENDERSON-SELLERS, A., KENNEDY, P. J. & WILSON, M. F. (1993) Biosphere–atmosphere transfer scheme (BATS) version 1e as coupled to the NCAR Community Climate Model. NCAR Tech. *Note, NCAR/TN387+ STR*.

ELTAHIR, E. A. B. (1996) El NiÃ±o and the natural variability in the flow of the Nile River. Water Resources Research, 32, 131-137.

ELTAYEB, G. E. (2003) Khartoum, Sudan. UN-HABITAT Case Studies, London, 2.

EMANUEL, K. (1991) A scheme for representing cumulus convection in large-scale models. Journal of the atmospheric sciences, 48, 2313–2335.

GIORGI, F., COPPOLA, E., SOLMON, F., MARIOTTI, L., SYLLA, M. B., BI, X., ELGUINDI, N., DIRO, G. T., NAIR, V. & GIULIANI, G. (2012) RegCM4: model description and preliminary tests over multiple CORDEX domains. Climate Research, 2, 7.

GIORGI, F., MARINUCCI, M. R. & BATES, G. T. (1993a) Development of a second-generation regional climate model (RegCM2). Part I: Boundary-layer and radiative transfer processes.

GRELL, G. A. (1993) Prognostic evaluation of assumptions used by cumulus parameterizations. *Monthly Weather Review;(United States),* 121.

HOLTSLAG, A. A. M., DE BRUIJN, E. I. F. & PAN, H. L. (1990) A high resolution air mass transformation model for short-range weather forecasting. *Monthly Weather Review,* 118.

Huffman, G. J., D. T. Bolvin, and R. F. Adler, 2011: GPCP Version 2.2 Combined Precipitation Data set., WDC-A, NCDC, Asheville, NC. Data set accessed October 2011 at http://www.ncdc.noaa.gov/oa/wmo/wdcamet-ncdc.html.

HUFFMAN, G. J., ADLER, R. F., MORRISSEY, M. M., BOLVIN, D. T., CURTIS, S., JOYCE, R., MCGAVOCK, B. & SUSSKIND, J. (2001) Global precipitation at one-degree daily resolution from multisatellite observations. Journal of Hydrometeorology, 2, 36-50.

JANSEN, E., OVERPECK, J., BRIFFA, K. R., DUPLESSY, J. C., JOOS, F., MASSON-DELMOTTE, V., OLAGO, D., OTTO-BLIESNER, B., PELTIER, W. R. & RAHMSTORF, S. (2007) Chapter 6. Palaeoclimate. *Climate Change 2007: The Physical Science Basis. Contribution of Working Group I to the Fourth Assessment Report of the Intergovernmental Panel on Climate Change***,** 443-498.

JURY, M. R. (2004) The coherent variability of African river flows: Composite climate structure and the Atlantic circulation. Water Sa, 29, 1-10.

Ji, L., and A. J. Peters, 2003: Assessing vegetation response to drought in the northern Great Plains using vegetation and drought indices, Remote Sens. Environ., 87(1), 85-98, doi: 10.1016/s0034-4257(03)00174-3.

KIEHL, J. T., HACK, J. J., BONAN, G. B. & BOVILLE, B. (1996) Description of the NCAR Community Climate Model(CCM 3). NASA.

Kogan, F. N., 1995: Droughts of the Late 1980s in the United States as Derived from NOAA Polar-Orbiting Satellite Data, Bull. Amer. Meteor. Soc., 76(5), 655-668, doi: 10.1175/1520-0477(1995)076<0655:dotlit>2.0.co;2.

LEE, T. & MCPHADEN, M. J. (2010) Increasing intensity of El NiÃ±o in the central-equatorial Pacific. Geophysical Research Letters, 37, L14603.

MEEHL, G. A., ARBLASTER, J. M., MATTHES, K., SASSI, F. & VAN LOON, H. (2009) Amplifying the Pacific climate system response to a small 11-year solar cycle forcing. Science, 325, 1114-1118.

Mckee, T. B., N. J. Doesken, and J. Kleist, 1993: The relationship of drought frequency and duration to time scales. Eight Conference on Applied Climatology, Anahaim, California, 179-184.

PAL, J. S., ELTAHIR, E. A. B. & SMALL, E. E. (2000) Simulation of regional-scale water and energy budgets- Representation of subgrid cloud and precipitation processes within RegCM. *Journal of geophysical research,* 105**,** 567–594.

PAL, J. S., GIORGI, F., BI, X., ELGUINDI, N., SOLMON, F., RAUSCHER, S. A., GAO, X., FRANCISCO, R., ZAKEY, A. & WINTER, J. (2007) Regional climate modeling for the developing world: the ICTP RegCM3 and RegCNET. *Bulletin of the American* Meteorological Society, 88, 1395-1409.

Pinzon, J. E., M. E. Brown, and C. J. Tucker, 2005: Satellite time series correction of orbital drift artifacts using empirical mode decomposition. Hilbert-Huang Transform: Introduction and Applications, N. Huang, Ed., 167-186.

POWER, S. B. & SMITH, I. N. (2007) Weakening of the Walker Circulation and apparent dominance of El NiÃ±o both reach record levels, but has ENSO really changed? Geophysical Research Letters, 34, L18702.

REYNOLDS, R. W., SMITH, T. M., LIU, C., CHELTON, D. B., CASEY, K. S. & SCHLAX, M. G. (2007) Daily high-resolution-blended analyses for sea surface temperature.

Sellers, P. J., 1985: Canopy reflectance, photosynthesis and transpiration, Int. J. Remote Sens., 6(8), 1335-1372, doi: 10.1080/01431168508948283.

SENEVIRATNE, S. I., NICHOLLS, N., EASTERLING, D., GOODESS, C. M., KANAE, S., KOSSIN, J., LUO, Y., MARENGO, J., MCINNES, K. & RAHIMI, M. (2012) Changes in climate extremes and their impacts on the natural physical environment. Managing the Risks of Extreme Events and Disasters to Advance Climate Change Adaptation, 109-230.

Tucker, C. J., J. E. Pinzon, and M. E. Brown, 2004: Global Inventory Modeling and Mapping Studies, NA94apr15b.n11-VIg, 92.90, Global Land Cover Facility, University of Maryland, College Park, Maryland, 04/15/1994.

Tucker, C. J., J. E. Pinzon, M. E. Brown, D. A. Slayback, E. W. Pak, R. Mahoney, E. F. Vermote, and N. El Saleous, 2005: An extended AVHRR 8-km NDVI dataset compatible with MODIS and SPOT vegetation NDVI data, *Int. J. Remote Sens.*, **26**(20), 4485-4498, doi: 10.1080/01431160500168686.

UPPALA, S., DEE, D., KOBAYASHI, S., BERRISFORD, P. & SIMMONS, A. (2008) Towards a climate data assimilation system: Status update of ERA-Interim. ECMWF Newsletter, 115, 12-18.

VECCHI, G. A. & WITTENBERG, A. T. (2010) El NiÃ±o and our future climate: where do we stand? Wiley Interdisciplinary Reviews: Climate Change, 1, 260-270.

WANG, G. & ELTAHIR, E. A. B. (1999) Use of ENSO information in medium-and long-range forecasting of the Nile floods. Journal of Climate, 12, 1726-1737.

WITTENBERG, A. T. (2009) Are historical records sufficient to constrain ENSO simulations? Geophysical Research Letters, 36, L12702.

YEH, S. W., KUG, J. S., DEWITTE, B., KWON, M. H., KIRTMAN, B. P. & JIN, F. F. (2009) El NiÃ±o in a changing climate. *Nature,* 461**,** 511-514.

6. APPENDICES

6.1 THE RAINFALL FOR EACH MEMBER DURING JJAS FOR 5 LA NINA YEAR, 5 EL NINO YEARS AND THE DIFFERENCE BETWEEN LA NINA YEARS AND EL NINO YEARS.

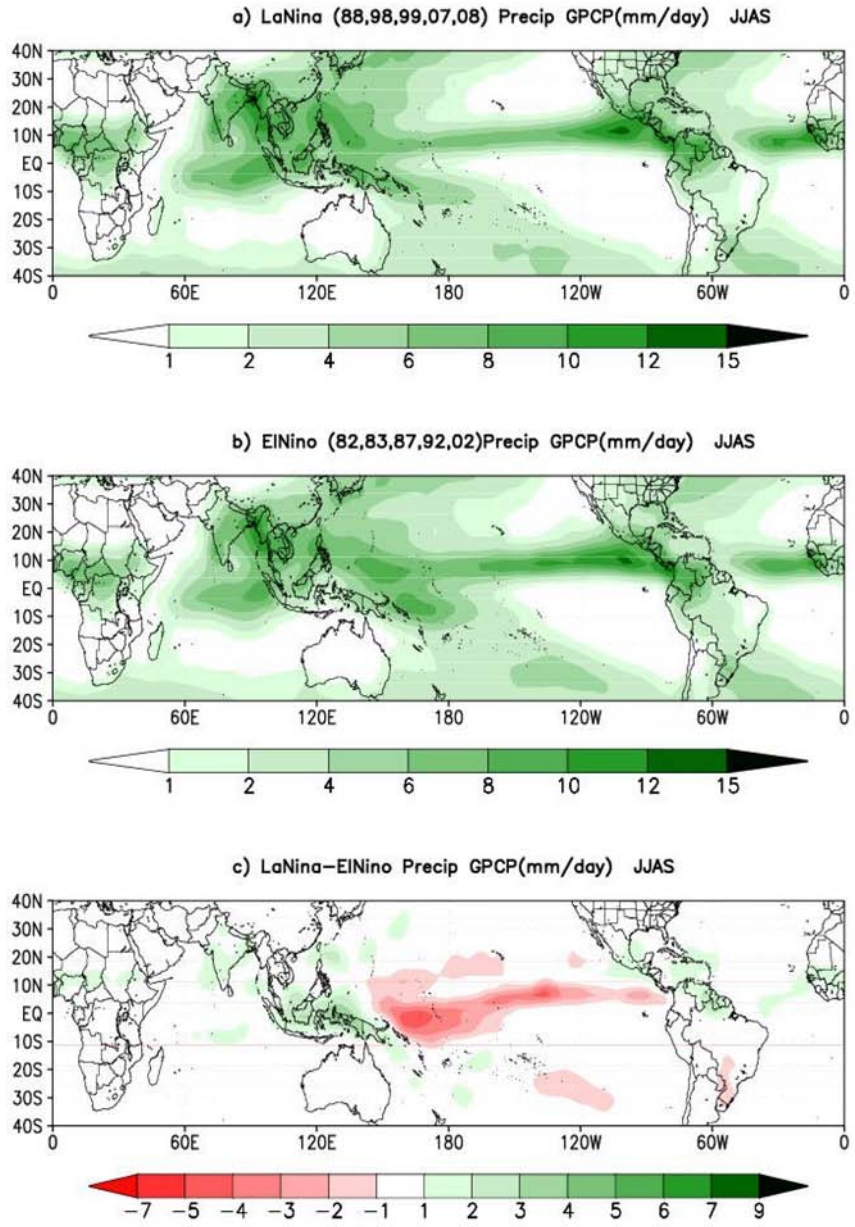

Figure 6.1: The rainfall for member 1 during JJAS for a) 5 La Nina years b) 5 El Nino years c) The difference between La Nina years and El Nino years.

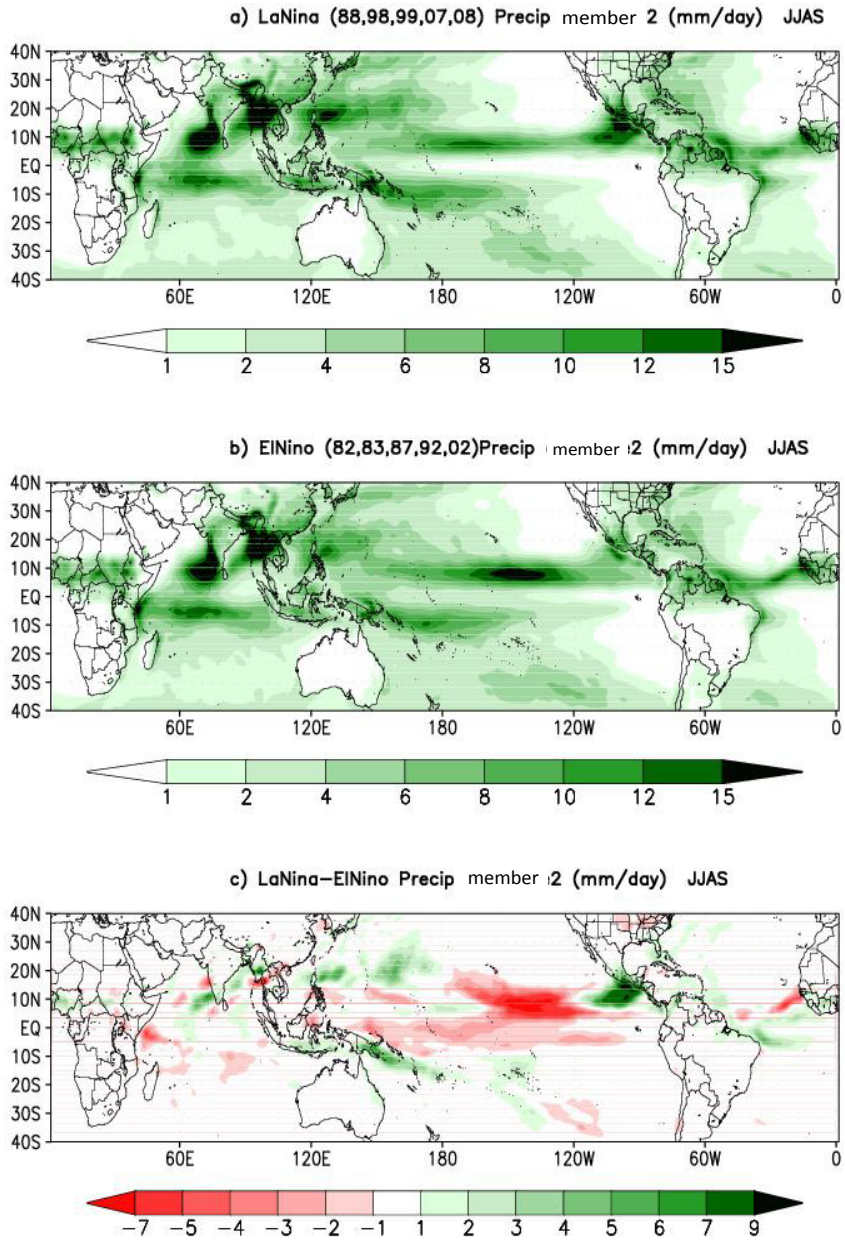

Figure 6.2: The rainfall for member 2 during JJAS for a) 5 La Nina years b) 5 El Nino years c) The difference between La Nina years and El Nino years.

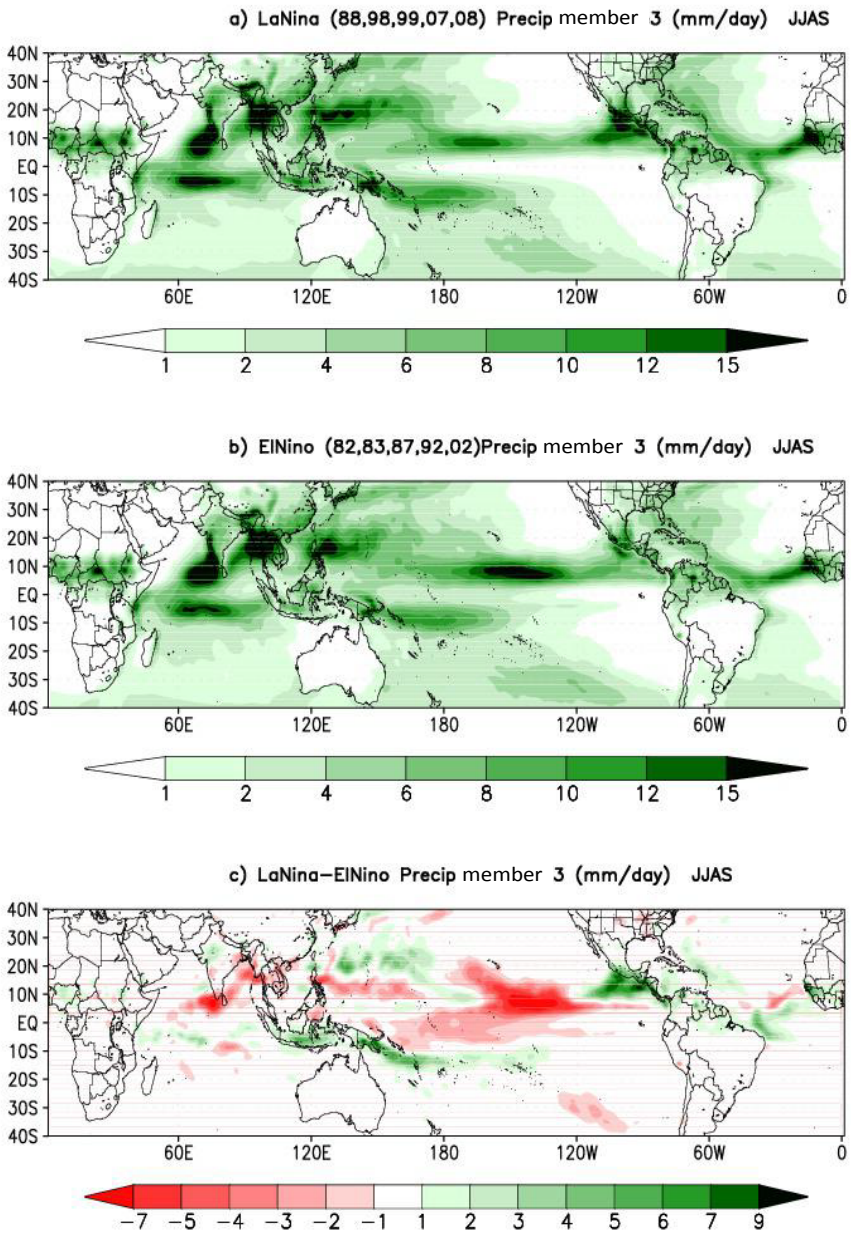

Figure 6.3: The rainfall for member 3 during JJAS for a) 5 La Nina years b) 5 El Nino years c) The difference between La Nina years and El Nino years.

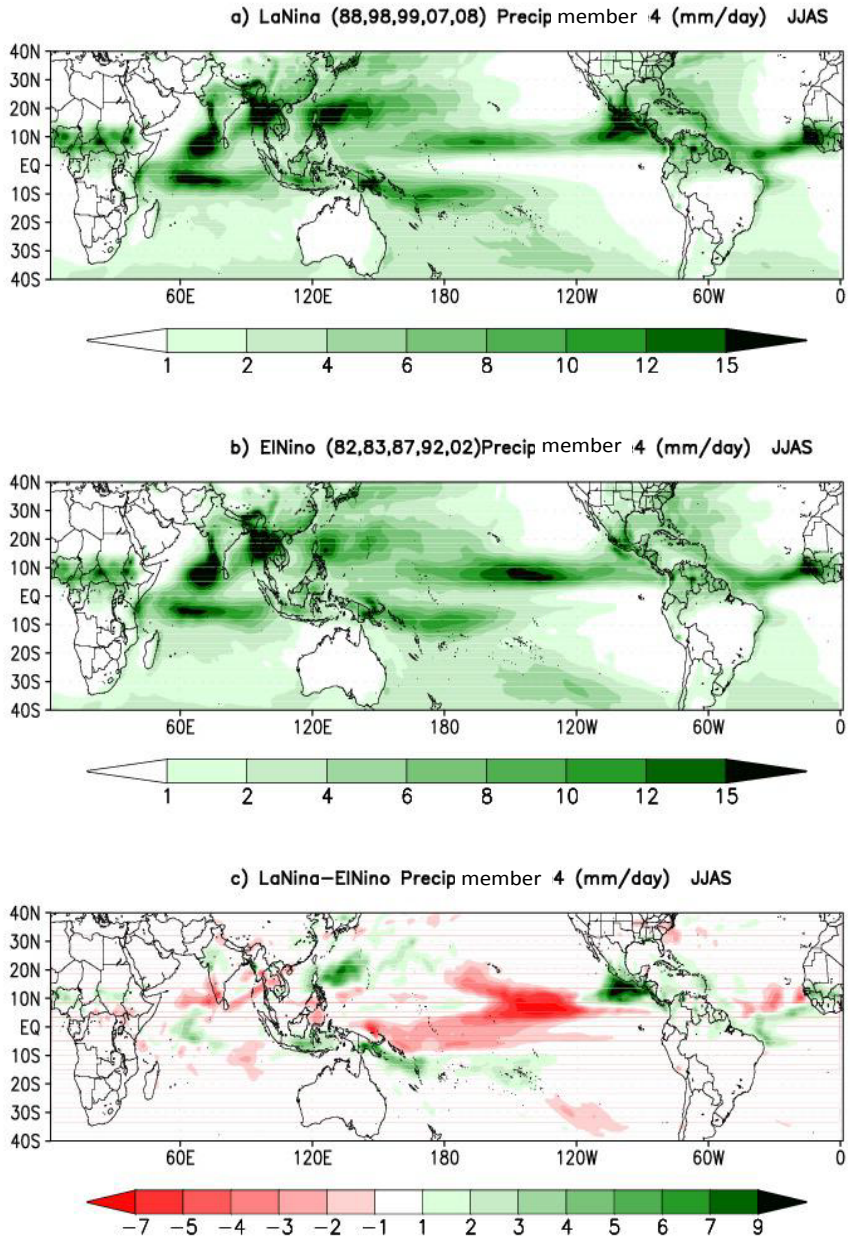

Figure 6.4: The rainfall for member 4 during JJAS for a) 5 La Nina years b) 5 El Nino years c) The difference between La Nina years and El Nino years.

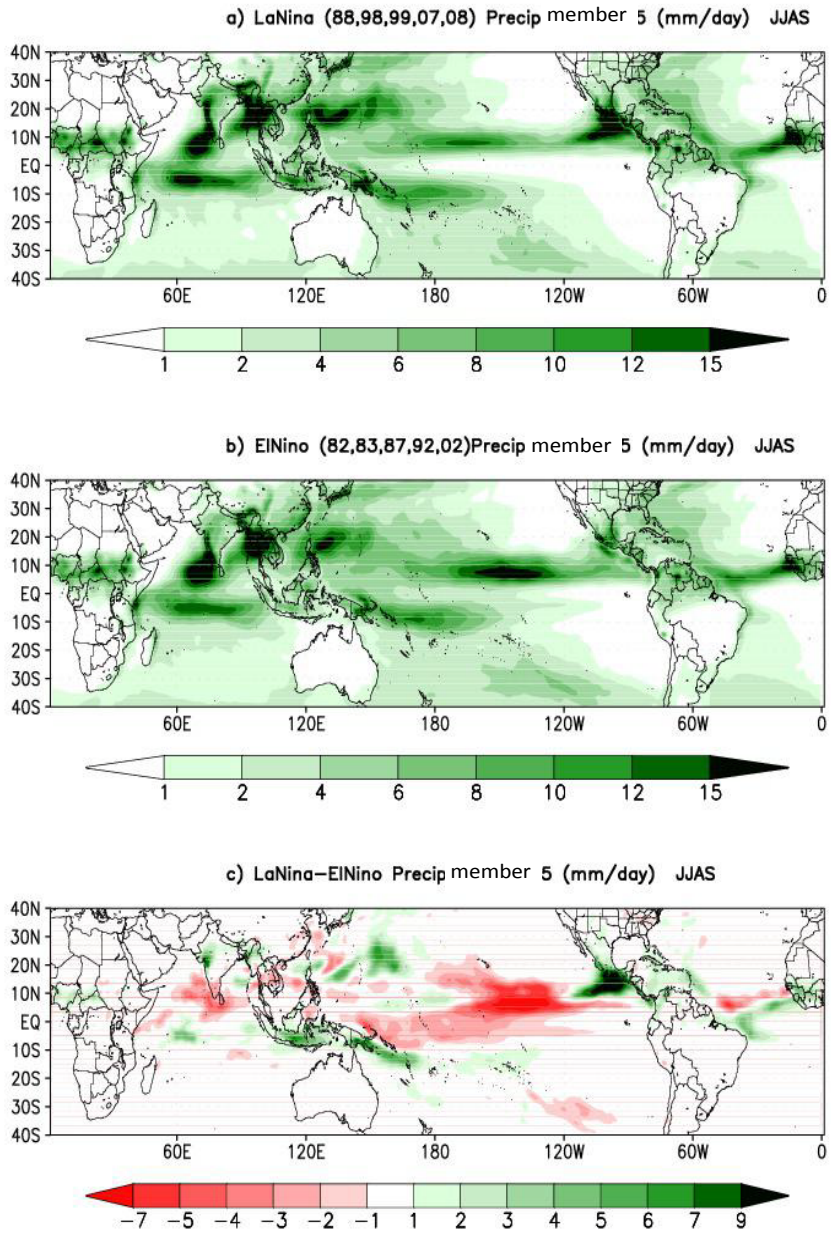

Figure 6.5: The rainfall for member 5 during JJAS for a) 5 La Nina years b) 5 El Nino years c) The difference between La Nina years and El Nino years.

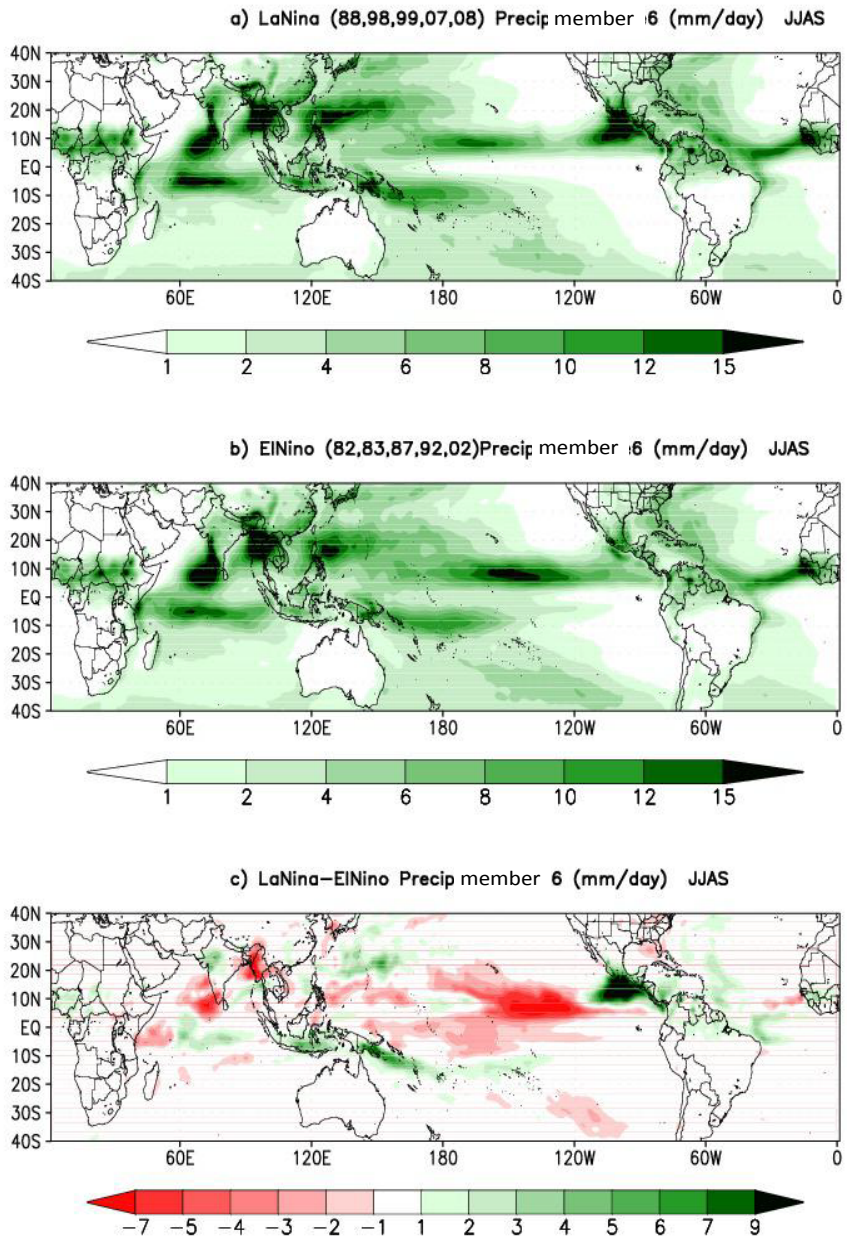

Figure 6.6: The rainfall for member 6 during JJAS for a) 5 La Nina years b) 5 El Nino years c) The difference between La Nina years and El Nino years.

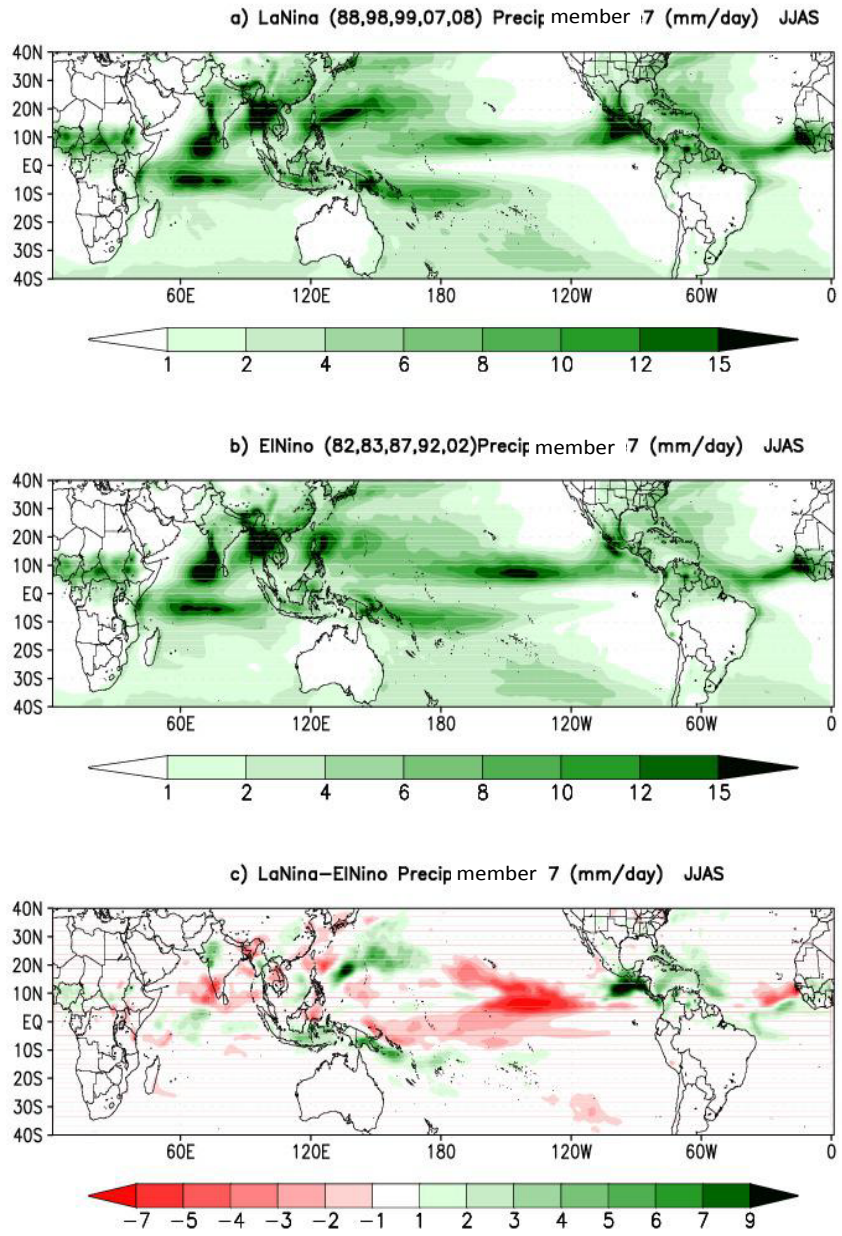

Figure 6.7: The rainfall for member 7 during JJAS for a) 5 La Nina years b) 5 El Nino years c) The difference between La Nina years and El Nino years.

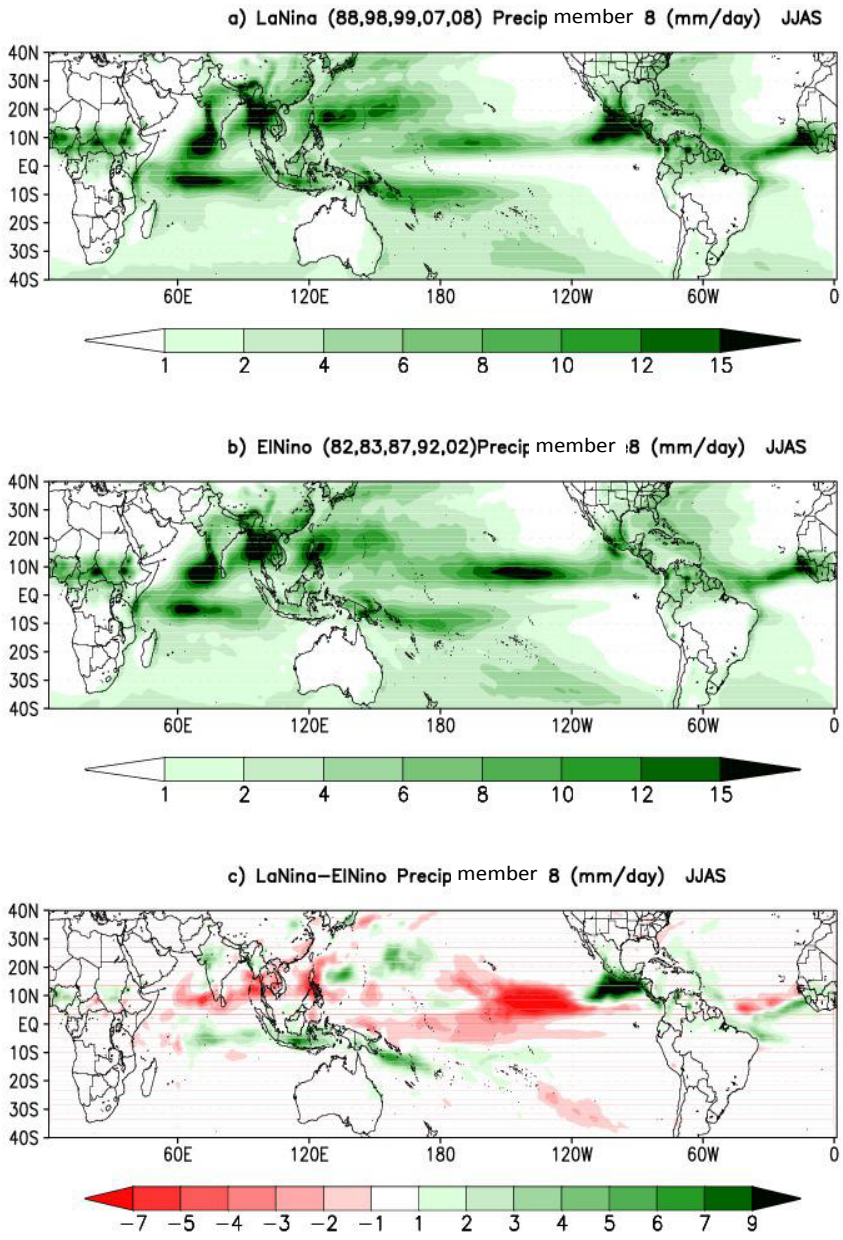

Figure 6.8: The rainfall for member 8 during JJAS for a) 5 La Nina years b) 5 El Nino years c) The difference between La Nina years and El Nino years.

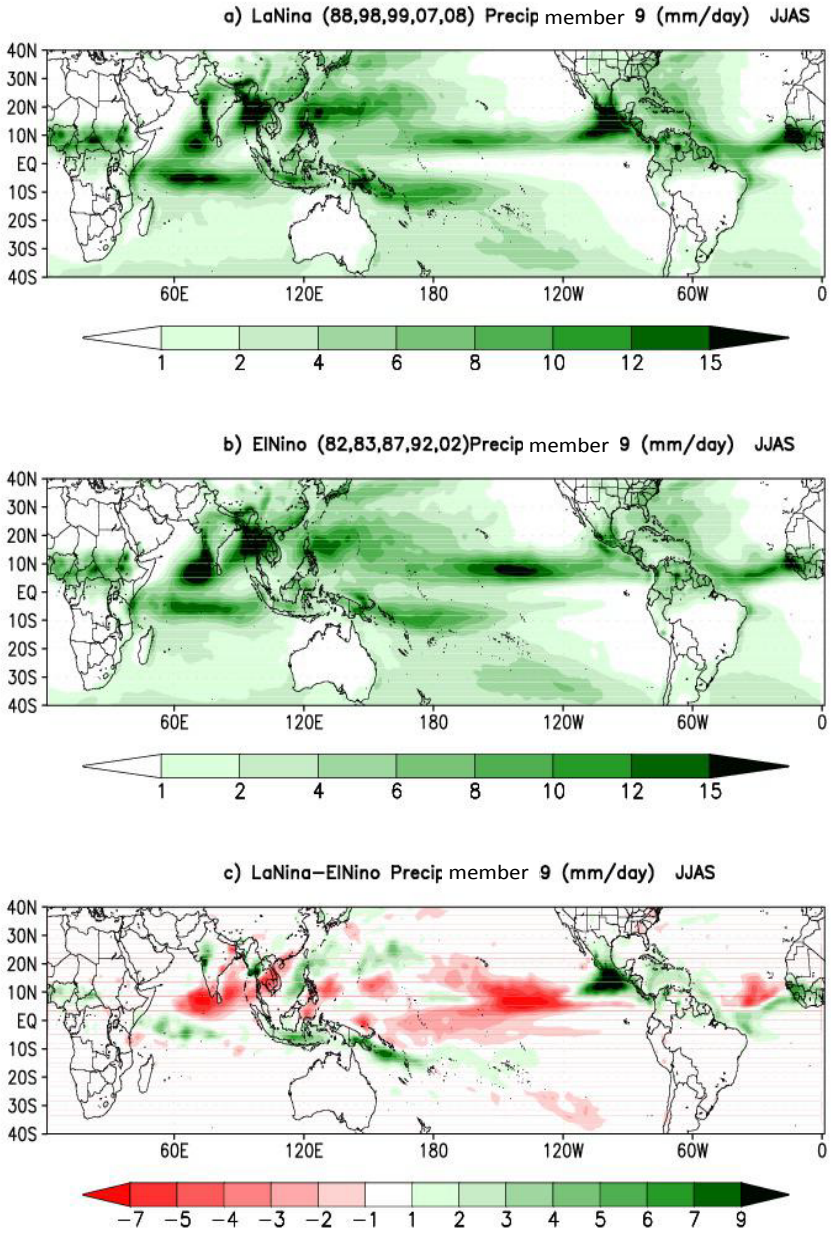

Figure 6.9: The rainfall for member 9 during JJAS for a) 5 La Nina years b) 5 El Nino years c) The difference between La Nina years and El Nino years.

6.2 THE CORRELATION FOR EACH MEMBER BETWEEN THE RAINFALL ANOMALIES OVER ETHIOPIAN HIGHLANDS AND THE SST ANOMALIES OVER THE PACIFIC OCEAN IN NINO 3.4 REGION.

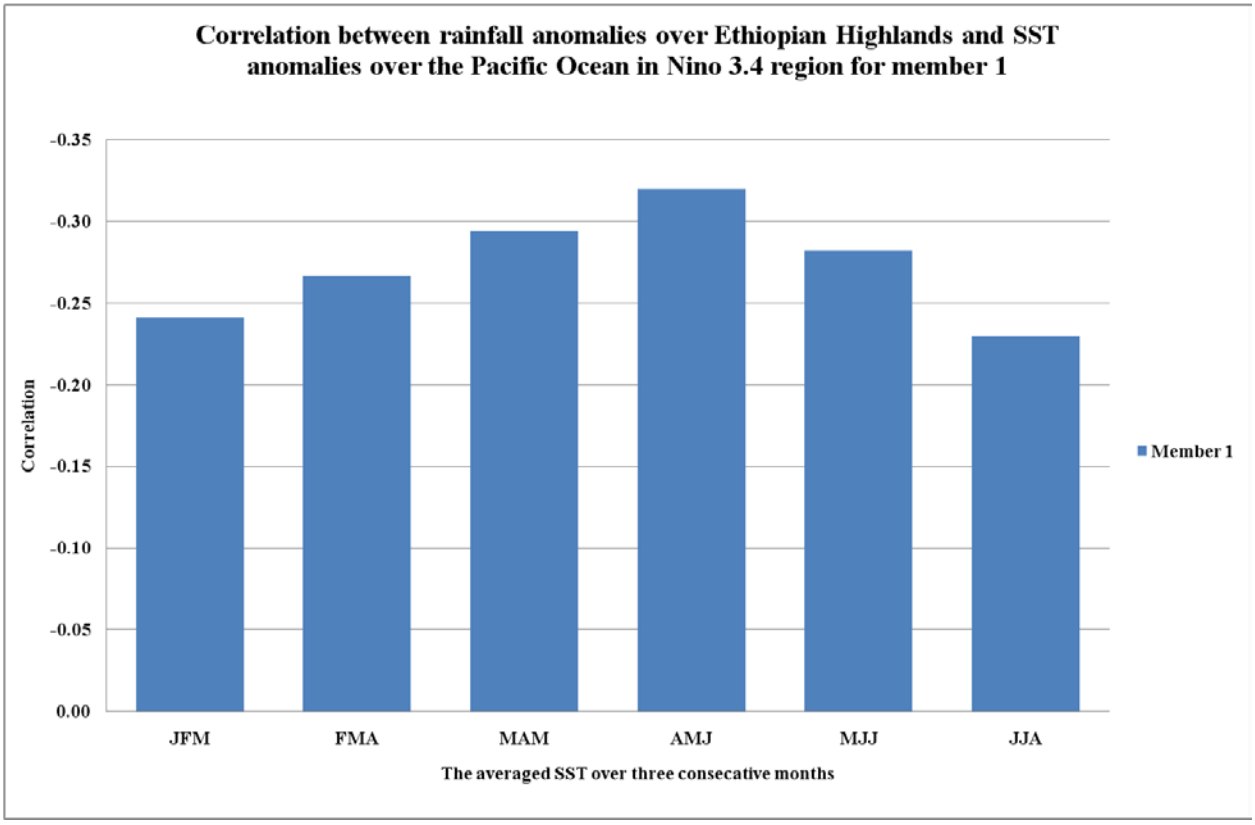

Figure 6.10: The correlation for member 1 between rainfall anomalies over Ethiopian Highlands for 9 averaged members and SST anomalies over the Pacific Ocean in Nino 3.4 region.

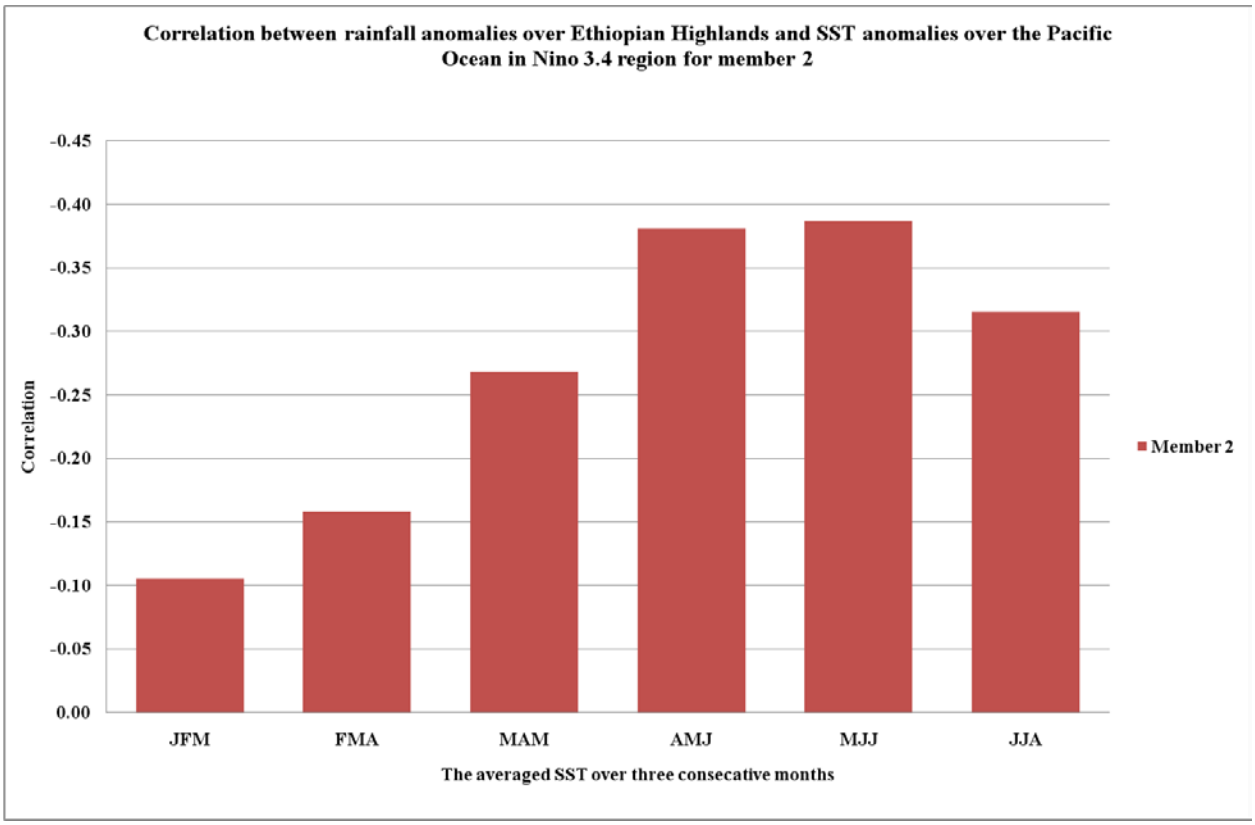

Figure 6.11: The correlation for member 2 between rainfall anomalies over Ethiopian Highlands for 9 averaged members and SST anomalies over the Pacific Ocean in Nino 3.4 region.

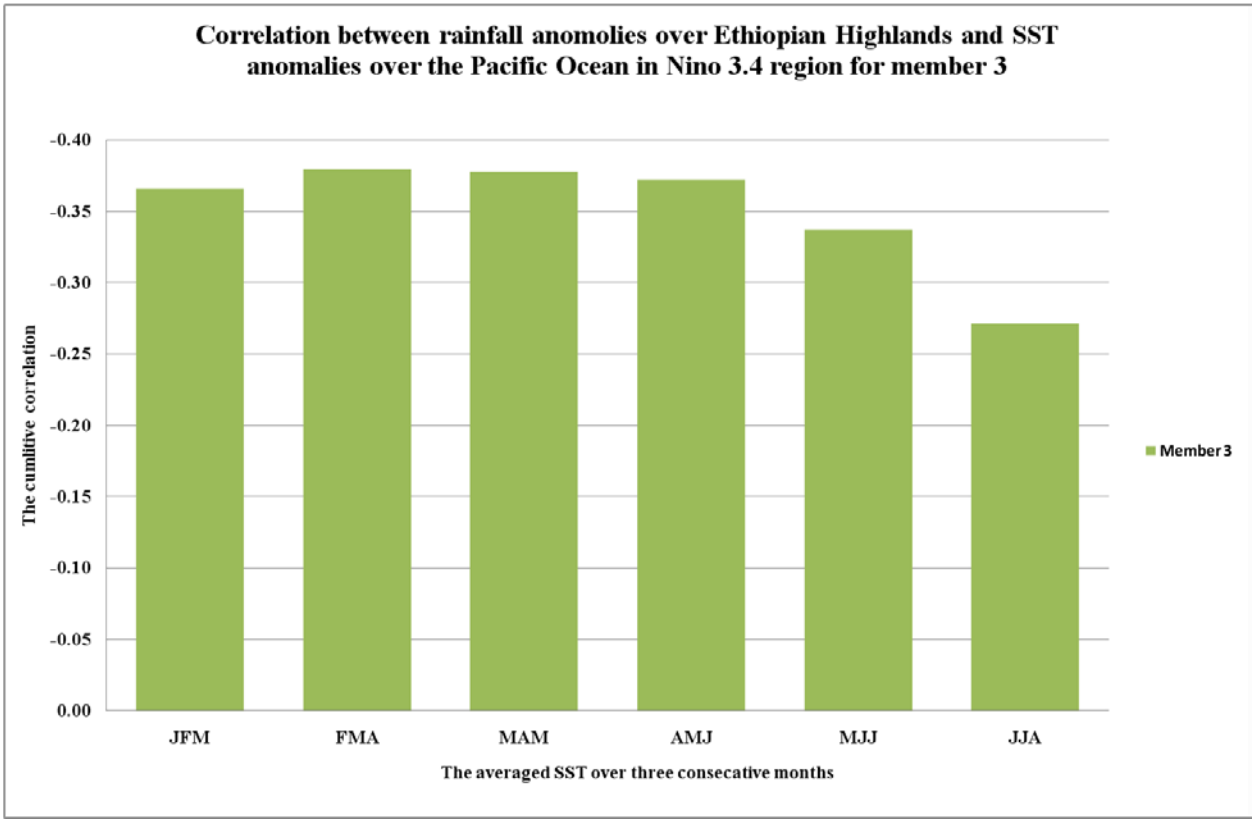

Figure 6.12: The correlation for member 3 between rainfall anomalies over Ethiopian Highlands for 9 averaged members and SST anomalies over the Pacific Ocean in Nino 3.4 region.

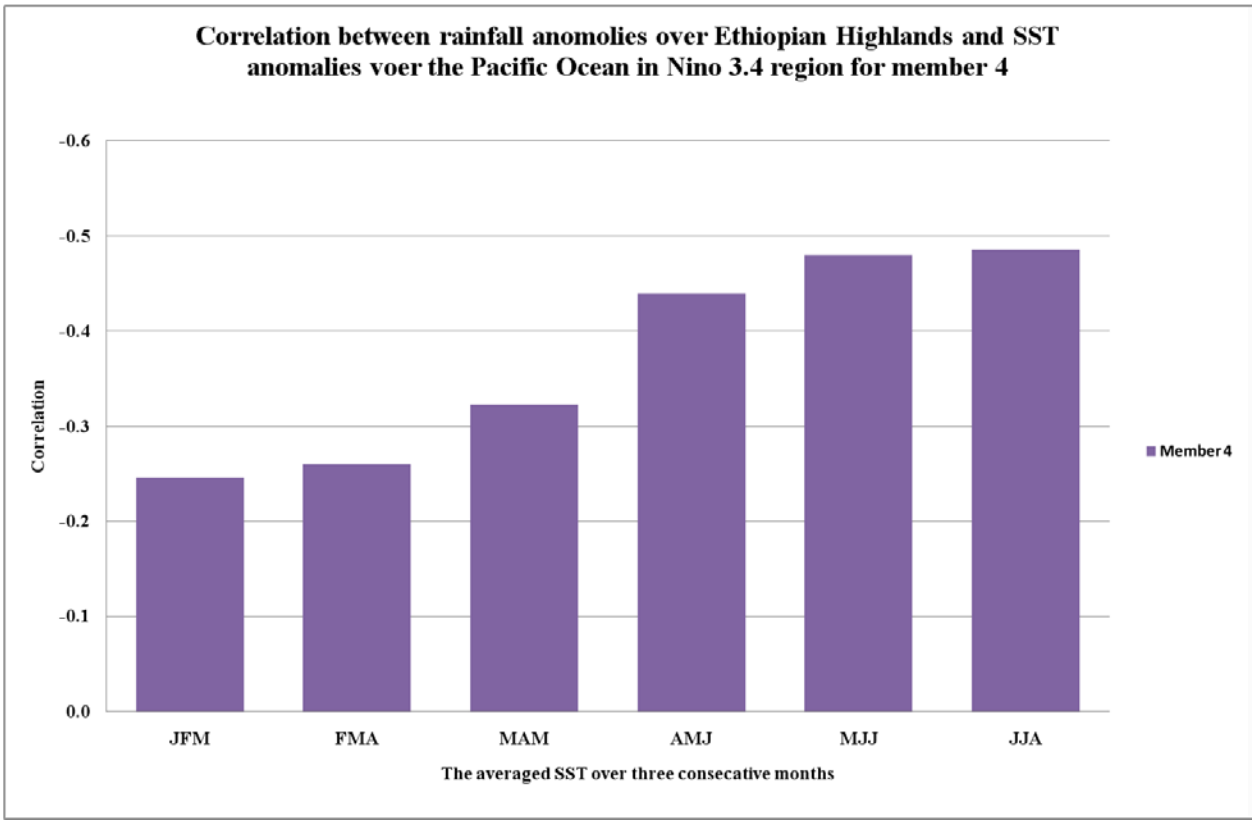

Figure 6.13: The correlation for member 4 between rainfall anomalies over Ethiopian Highlands for 9 averaged members and SST anomalies over the Pacific Ocean in Nino 3.4 region.

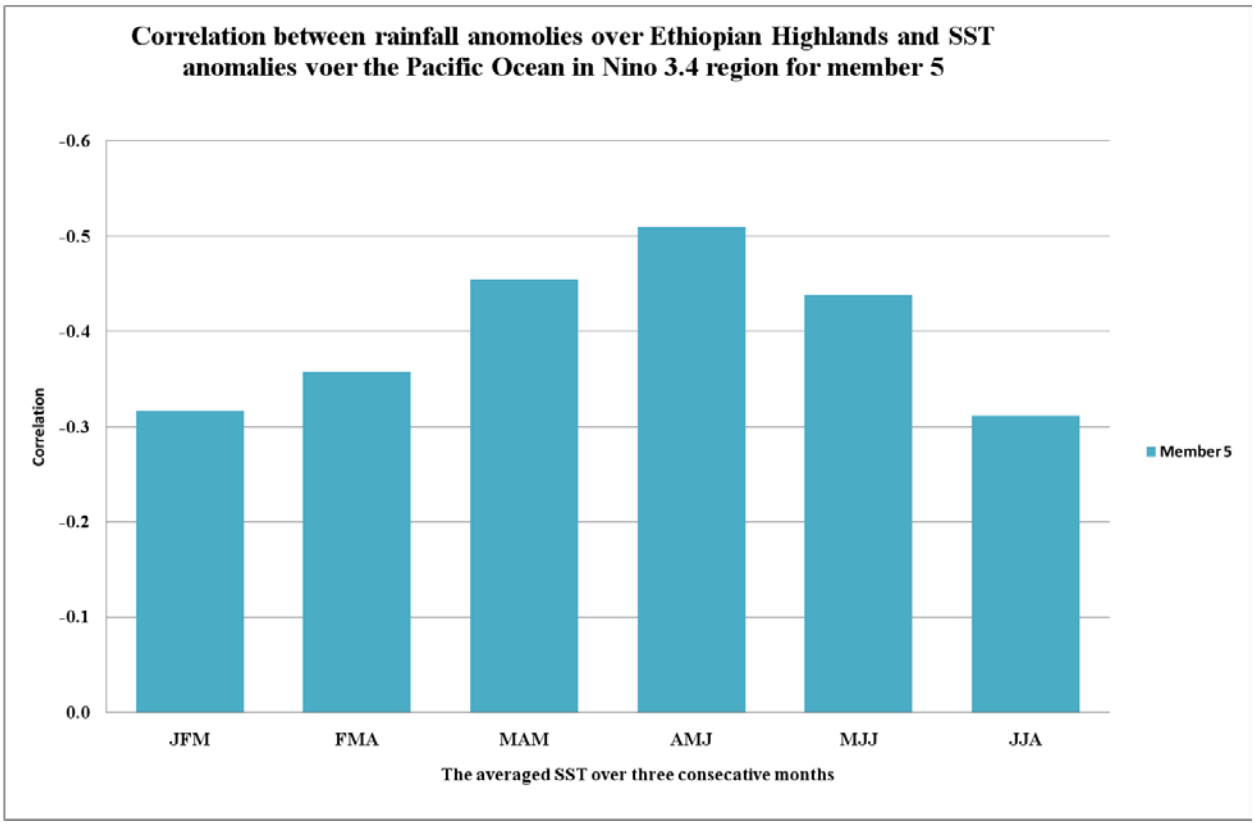

Figure 6.14: The correlation for member 5 between rainfall anomalies over Ethiopian Highlands for 9 averaged members and SST anomalies over the Pacific Ocean in Nino 3.4 region.

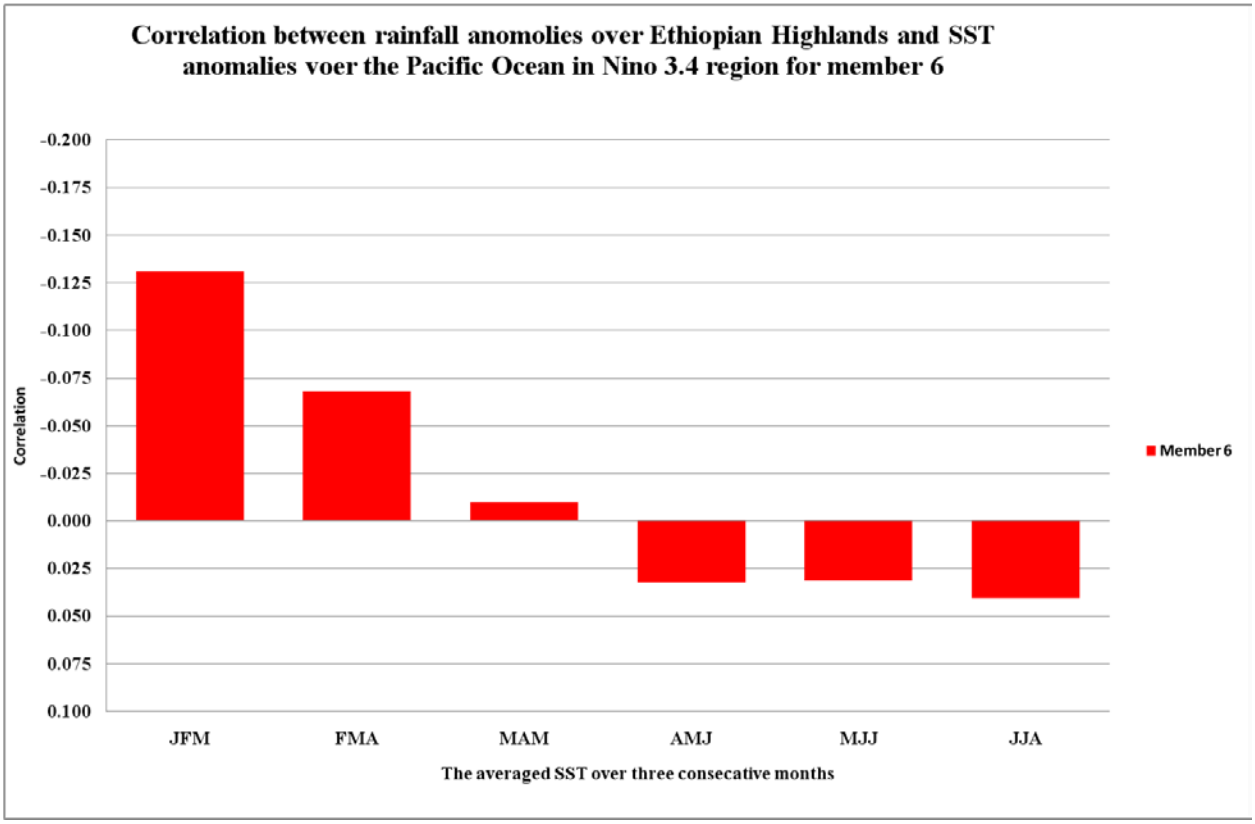

Figure 6.15: The correlation for member 6 between rainfall anomalies over Ethiopian Highlands for 9 averaged members and SST anomalies over the Pacific Ocean in Nino 3.4 region.

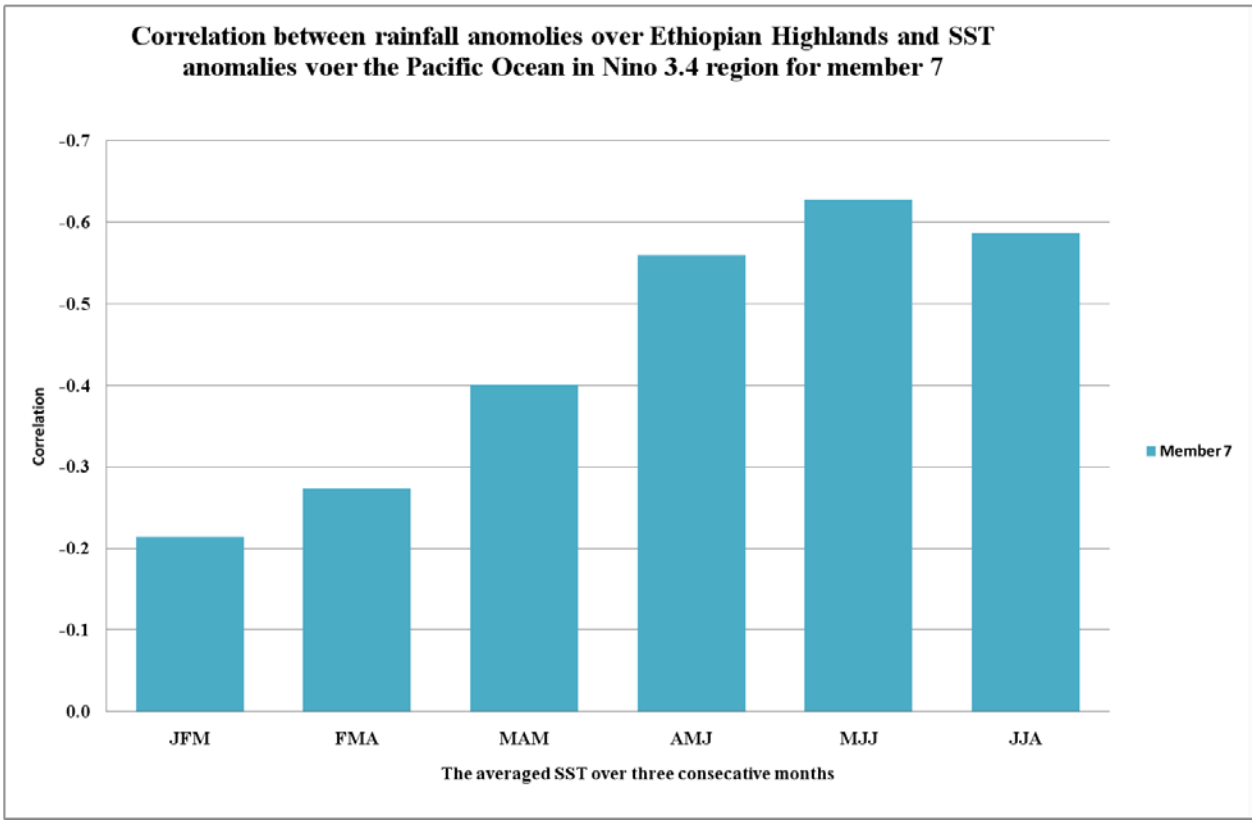

Figure 6.16: The correlation for member 7 between rainfall anomalies over Ethiopian Highlands for 9 averaged members and SST anomalies over the Pacific Ocean in Nino 3.4 region.

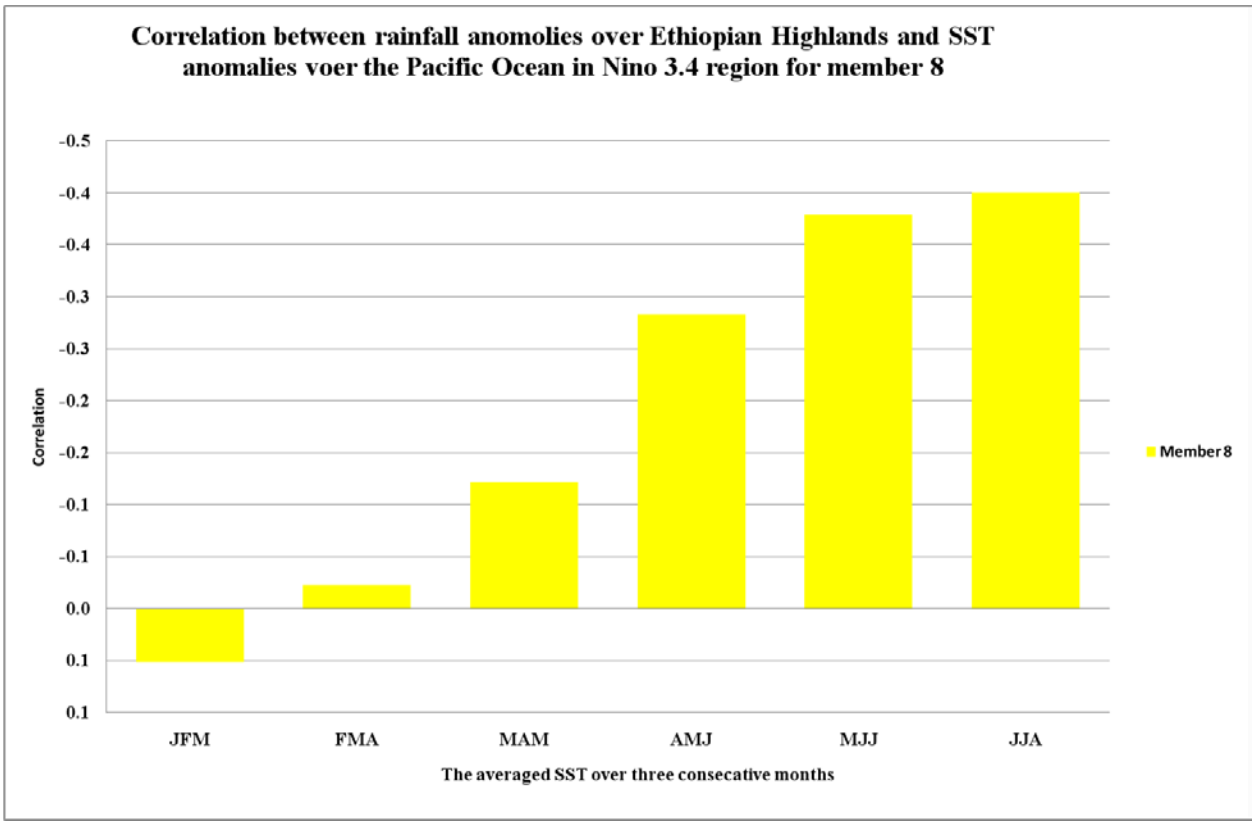

Figure 6.17: The correlation for member 8 between rainfall anomalies over Ethiopian Highlands for 9 averaged members and SST anomalies over the Pacific Ocean in Nino 3.4 region.

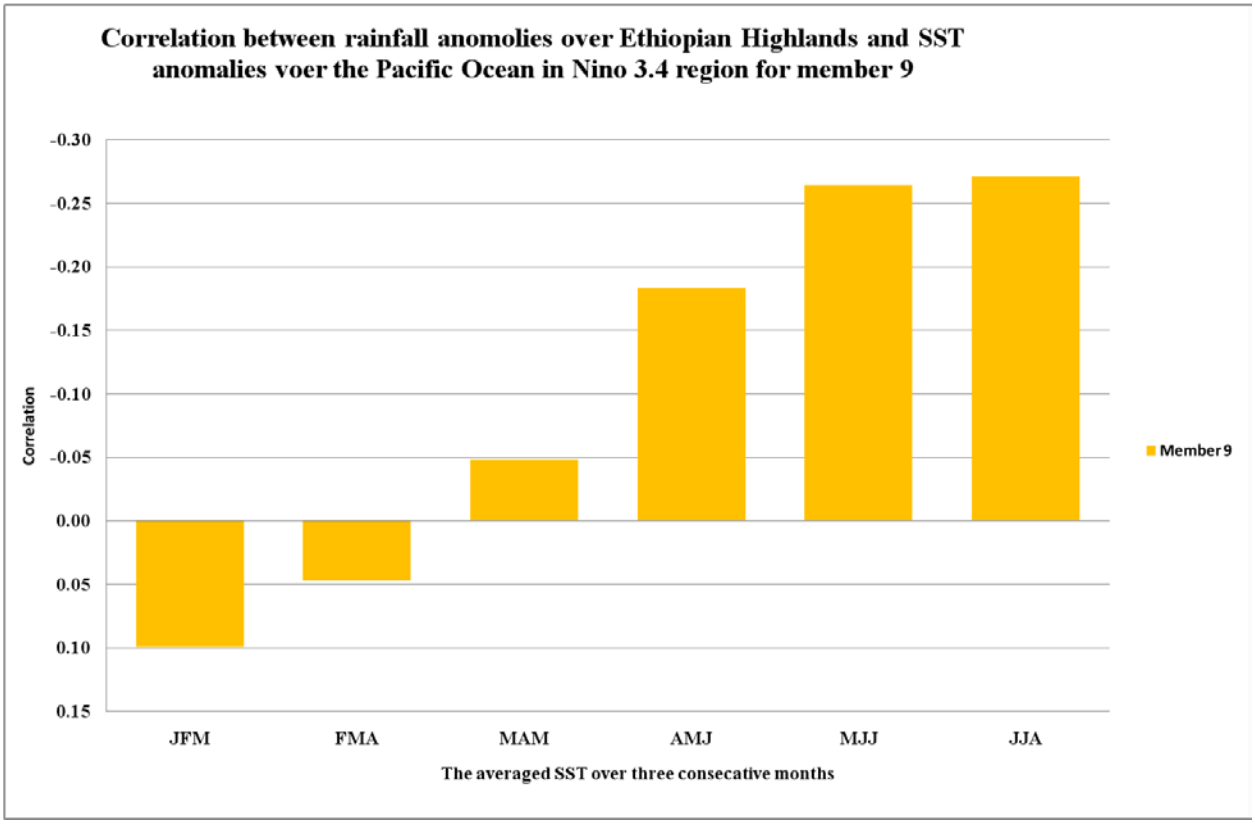

Figure 6.18: The correlation for member 9 between rainfall anomalies over Ethiopian Highlands for 9 averaged members and SST anomalies over the Pacific Ocean in Nino 3.4 region.

6.3 THE SST ANOMALIES DURING DIFFERENT SEASONS IN NINO 3.4 REGION AND THE RAINFALL ANOMALIES IN THE UPPER CATCHMENT OF THE BLUE NILE FOR EACH MEMBER.

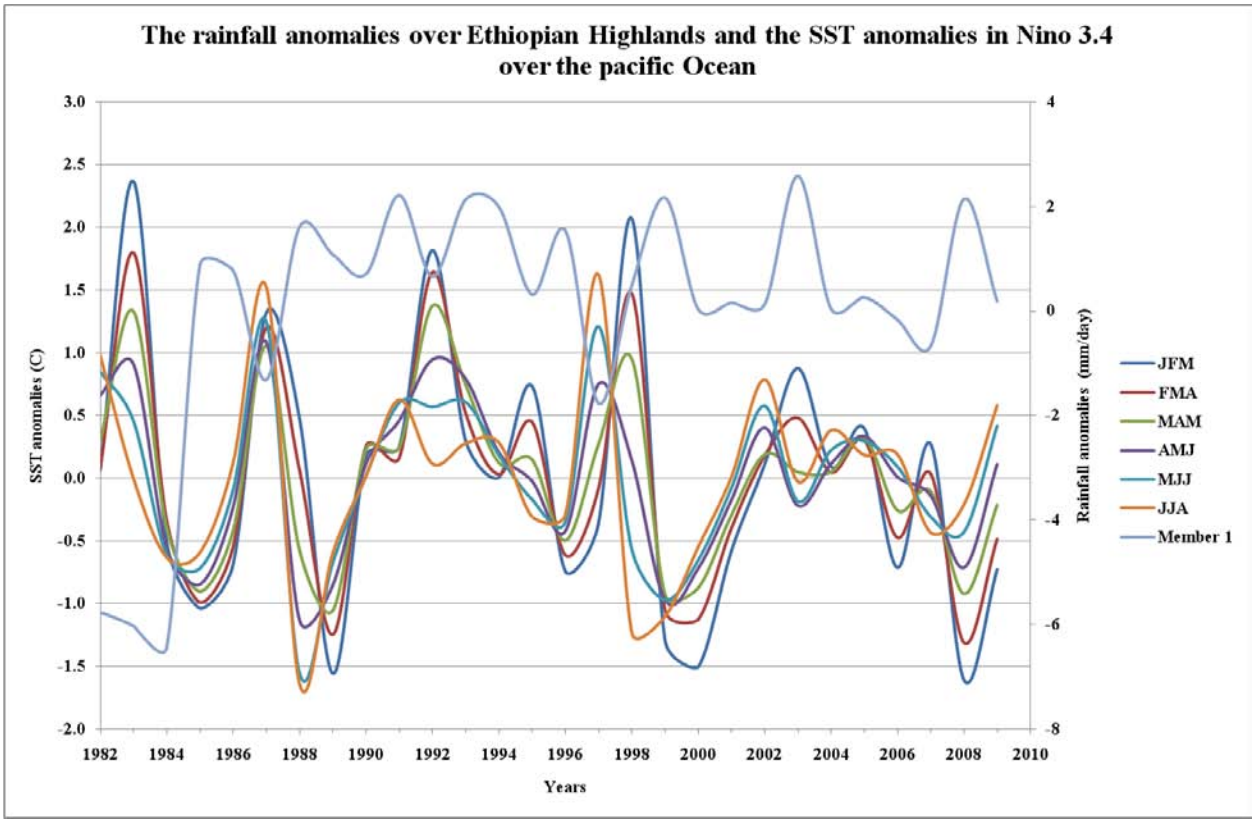

Figure 6.19: The SST anomalies during different seasons in Nino 3.4 region and the rainfall anomalies in the upper catchment of the Blue Nile for member 1.

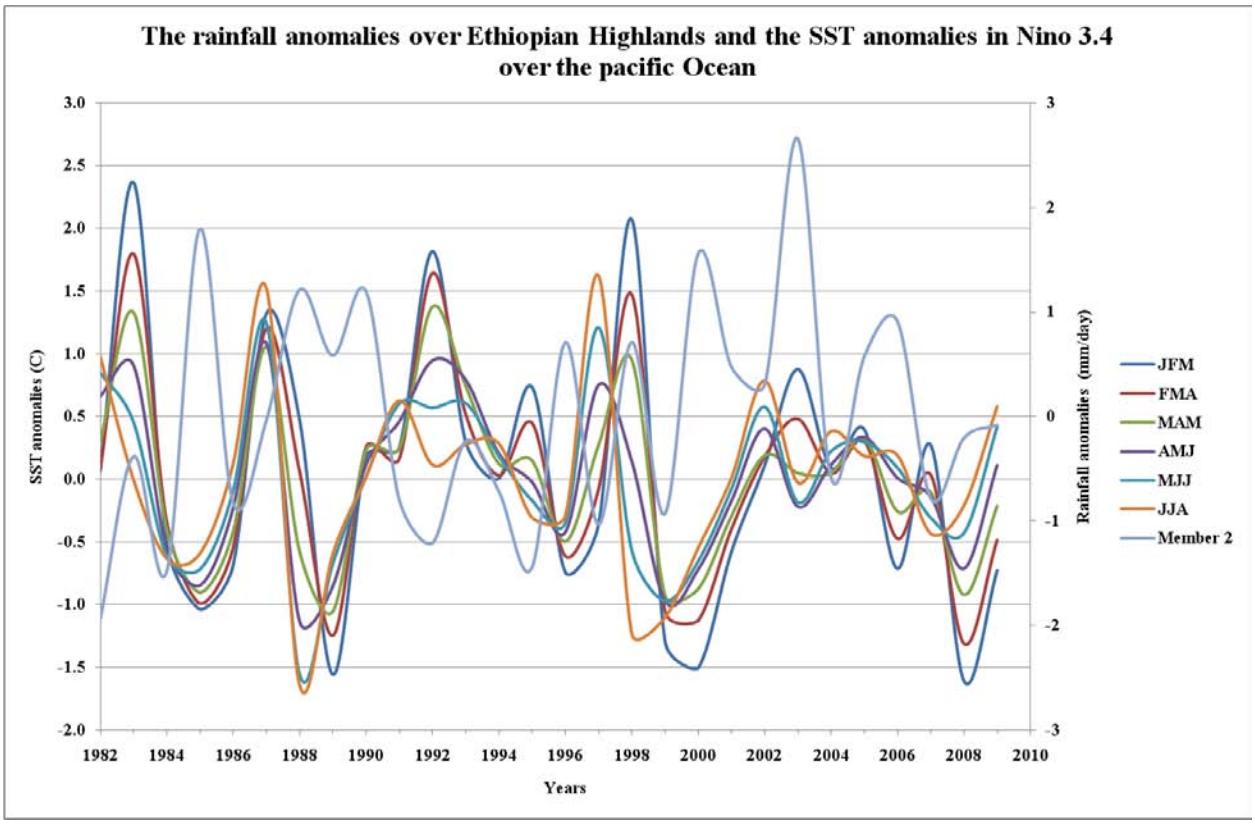

Figure 6.20: The SST anomalies during different seasons in Nino 3.4 region and the rainfall anomalies in the upper catchment of the Blue Nile for member 2.

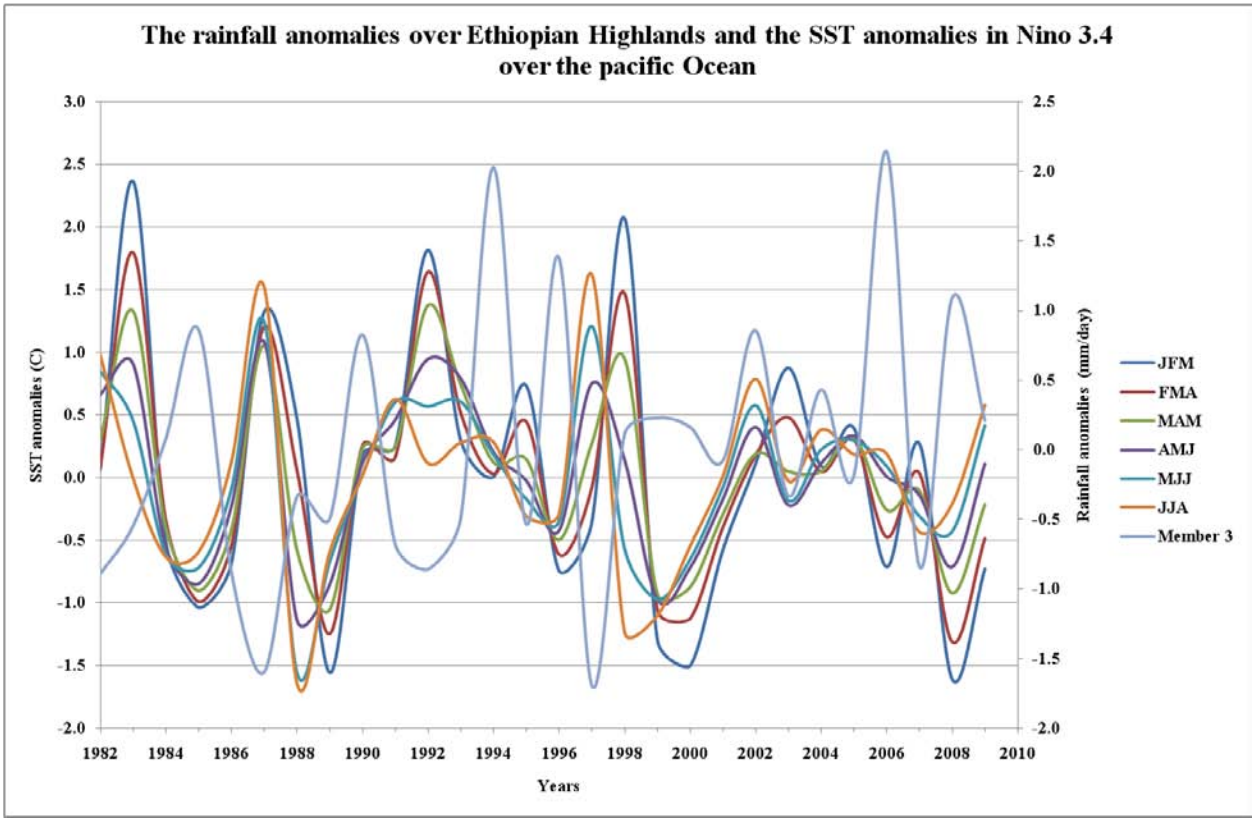

Figure 6.21: The SST anomalies during different seasons in Nino 3.4 region and the rainfall anomalies in the upper catchment of the Blue Nile for member 3.

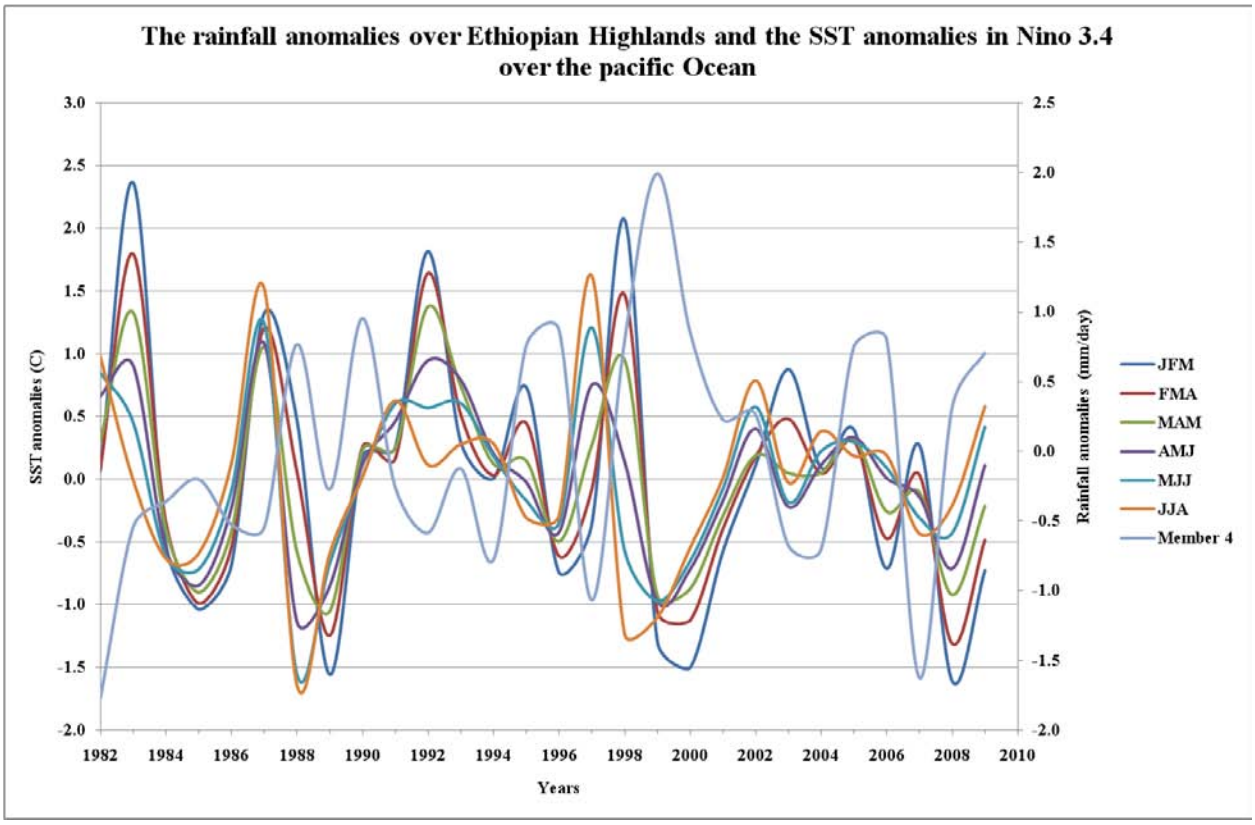

Figure 6.22: The SST anomalies during different seasons in Nino 3.4 region and the rainfall anomalies in the upper catchment of the Blue Nile for member 4.

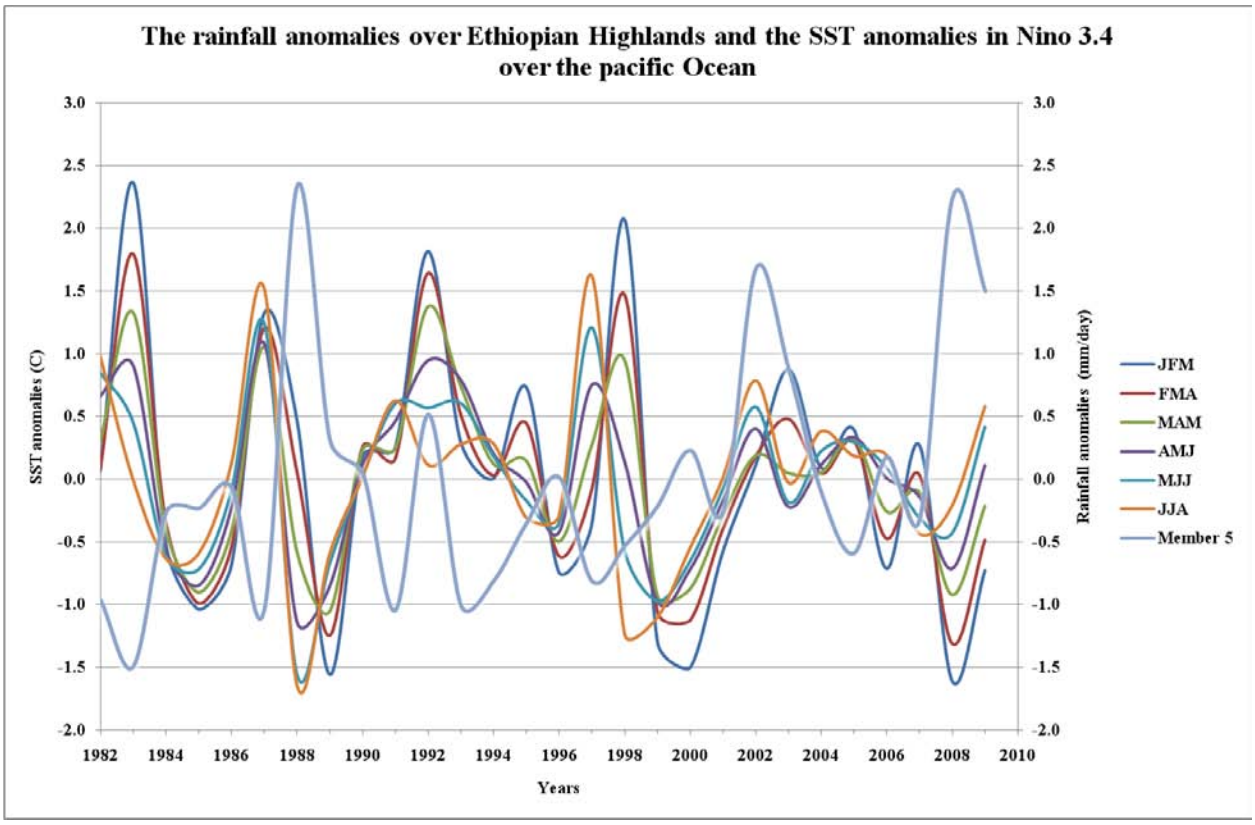

Figure 6.23: The SST anomalies during different seasons in Nino 3.4 region and the rainfall anomalies in the upper catchment of the Blue Nile for member 5.

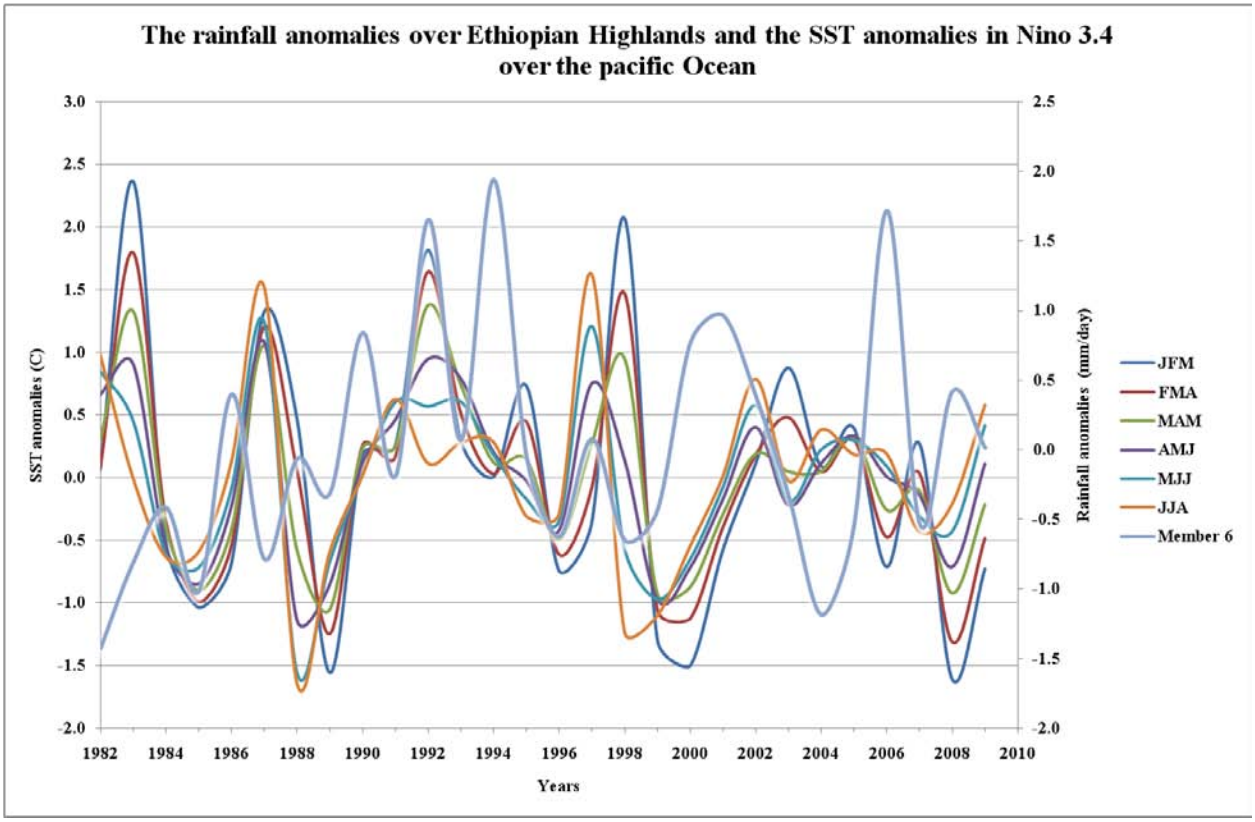

Figure 6.24: The SST anomalies during different seasons in Nino 3.4 region and the rainfall anomalies in the upper catchment of the Blue Nile for member 6.

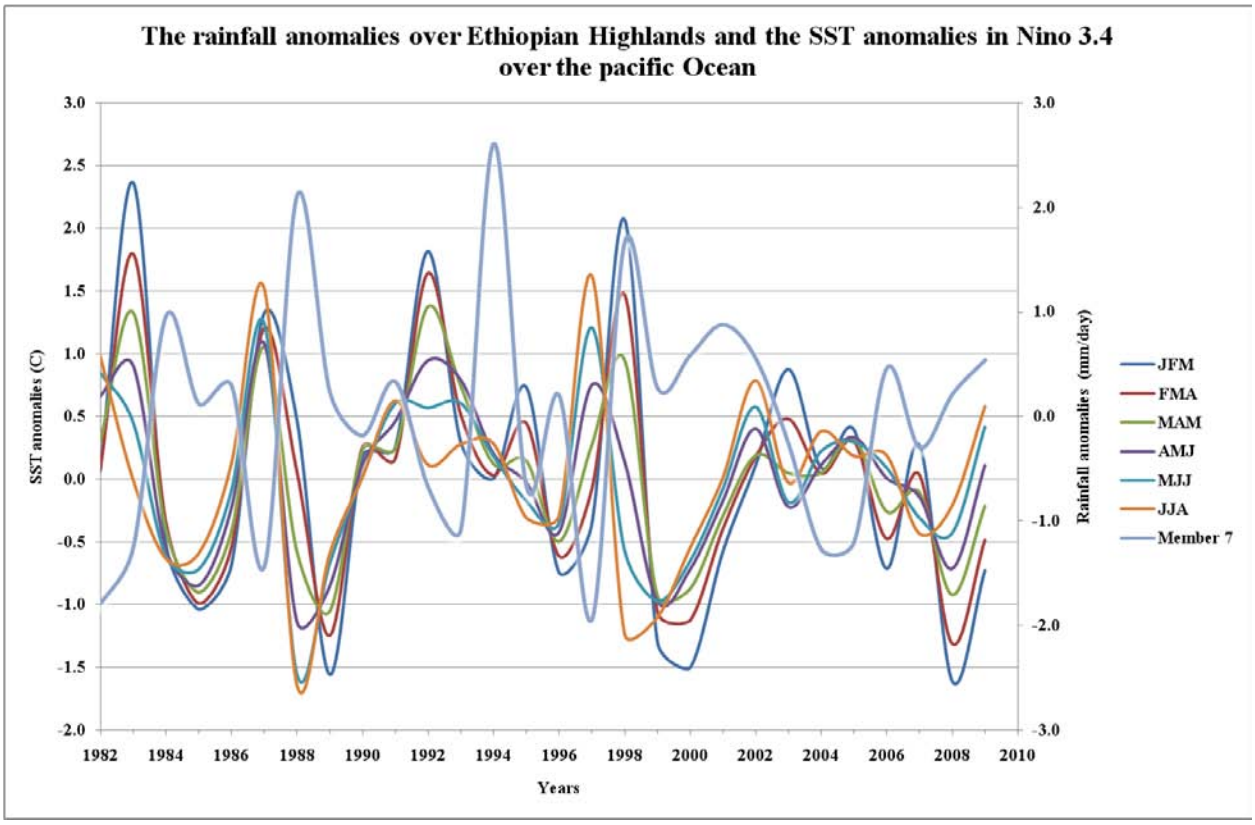

Figure 6.25: The SST anomalies during different seasons in Nino 3.4 region and the rainfall anomalies in the upper catchment of the Blue Nile for member 7.

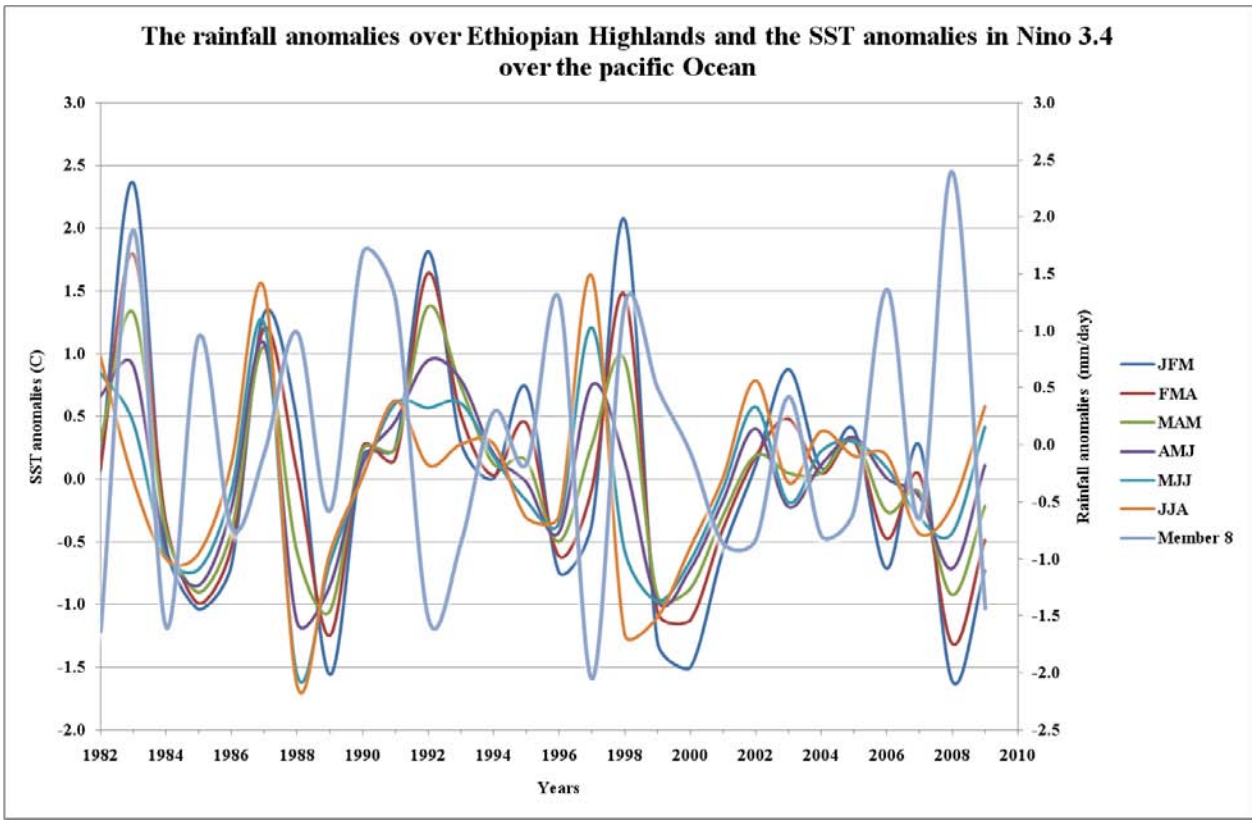

Figure 6.26: The SST anomalies during different seasons in Nino 3.4 region and the rainfall anomalies in the upper catchment of the Blue Nile for member 8.

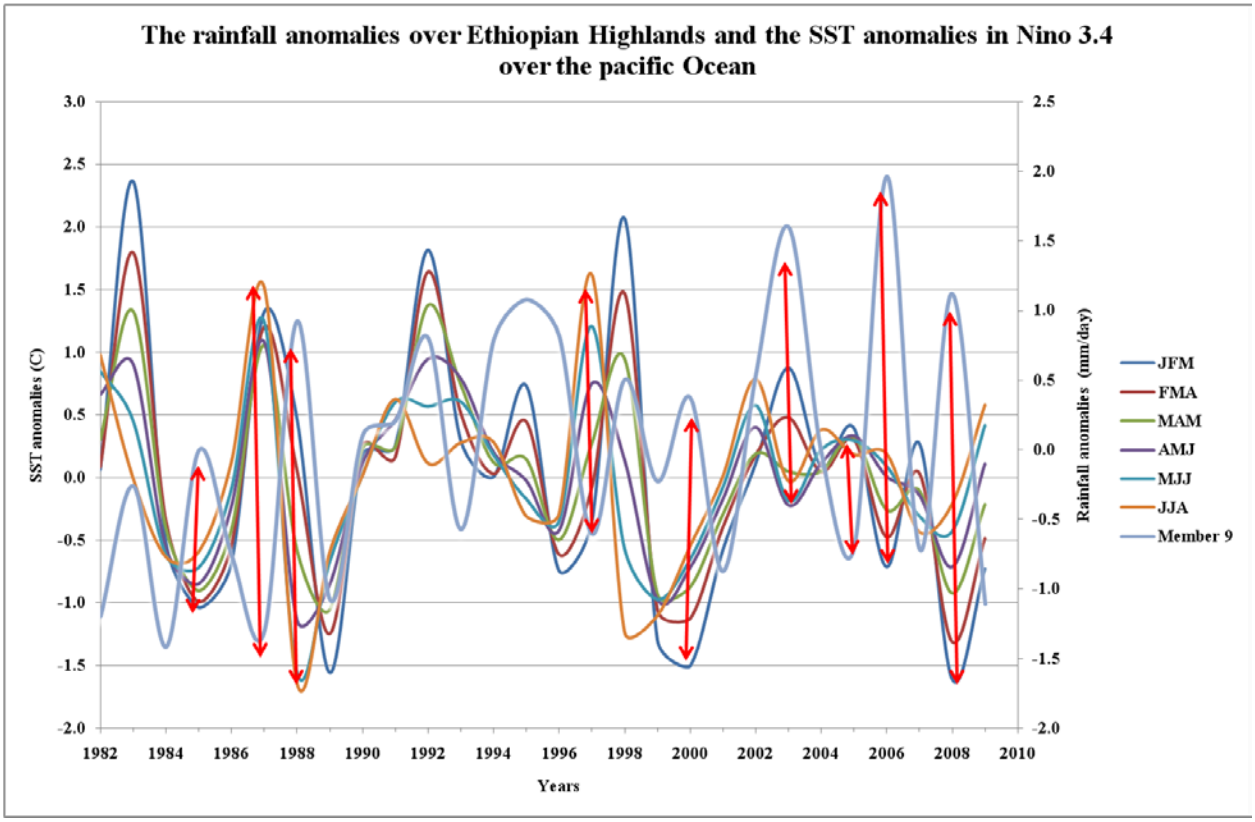

Figure 6.27: The SST anomalies during different seasons in Nino 3.4 region and the rainfall anomalies in the upper catchment of the Blue Nile for member 9.